

Thrust Performance Dependency On Propellant Characteristic of Ablation-Fed Pulsed Plasma Thruster

齊木, 淳
九州大学大学院総合理工学府先端エネルギー理工学専攻

<https://hdl.handle.net/2324/4067220>

出版情報：九州大学, 2019, 修士, 修士
バージョン：
権利関係：



令和元年度
九州大学大学院 総合理工学府
先端エネルギー理工学専攻
修士論文

論文名

Thrust Performance Dependency On Propellant
Characteristic of Ablation-Fed Pulsed Plasma Thruster

氏名

齊木 淳

指導教員名

山本 直嗣

<u>CONTENT</u>	III
CHAPTER 1: INTRODUCTION	1
1.1 WHAT IS THE ELECTRIC PROPULSION	1
1.2. RESEARCH BACKGROUND	2
1.3. THE OBJECTIVE OF THIS RESEARCH	4
1.4. PULSED PLASMA THRUSTER	4
1.5. PPT TYPES	7
1.6. PPT MODELS	8
1.6.1. THE MODEL APPLYING LCR CIRCUIT	8
1.6.2. THE MODEL APPLYING MHD THEORY	15
1.6.3. THE MODEL APPLYING ELECTROTHERMAL ACCELERATION	18
CHAPTER 2: EXPERIMENTAL EQUIPMENT	20
2.1. EXPERIMENT SYSTEM	20
2.2. MEASUREMENT AND CONTROL EQUIPMENT	21
2.2.1. THRUST SIGNAL RECEIVER AND IGNITER SIGNAL GENERATOR	22
2.2.2. ROGOWSKI COIL	22
2.2.3. DISCHARGE CURRENT AND VOLTAGE WAVEFORM MEASUREMENT	26
2.3. POWER SUPPLY	27
2.3.1. POWER SUPPLY FOR PPT	27
2.3.2. IGNITER MODULE	27
2.4. THRUST MEASURING SYSTEM	29
2.4.1 THRUSTER STAND	29
2.4.2 CALIBRATION	30
2.5. VACUUM SYSTEM	33
2.6. HIGH SPEED CAMERA (FASTCAM SA-Z)	35
CHAPTER 3: PERFORATED SOLID PROPELLANT VERIFICATION	36
3.1. LABORATORY PPT	36
3.2. NORMAL SHAPE SOLID PROPELLANT TEST	37
3.2.1 NORMAL SHAPE PTFE SOLID PROPELLANT EXPERIMENT	37
3.2.2 RESULT AND DISCUSSION	40
3.3. PERFORATED SOLID PROPELLANT TEST	45

3.3.1 PERFORATED SOLID PROPELLANT	45
3.3.2 PERFORATED SOLID PROPELLANT RESULT AND DISCUSSION.....	46
3.3.3 COMPARISON OF PERFORATED AND NORMAL SHAPE SOLID PROPELLANT.....	49
CHAPTER 4: CONCLUSION.....	54
REFERENCES	56
ACKNOWLEDGEMENTS	59

Chapter 1: Introduction

In this chapter, the brief introduction concerning the background research and research background and the motivation of the thesis will be presented. The literature review will be conducted in order to explain the main concepts presented in this paper.

1.1. What is the electric propulsion?

In general, the propulsion unit is normally the chemical rocket engine which is installed on launch vehicle. The thrust of chemical propulsion unit is generated due to the increasing enthalpy per unit time caused by the burning fuels and oxidants. Different from the chemical propulsion unit, the electric propulsion unit generates a thrust due to the electric power such as electrothermal, electromagnetic and electrostatic. The limitations of available thrust of chemical propulsion are dependent on specific chemical energy of the fuel. In contrast, the electric propulsion unit can generate thrust unlimitedly according to the supply power theoretically. The primary characteristic differences of both propulsions are summarized in Table 1.1. Due to their different characteristics, the chemical propulsion is normally applied to launch vehicle, and electric propulsion is applied to satellite.

Table 1.1. Differences of chemical and electric propulsion units

	Chemical	Electric
Thrust per unit time	High	Low
Thrust efficiency	Low	High

Propulsion unit is basically evaluated by specific impulse I_{sp} or momentum coupling coefficient C_m . The specific impulse is basically applied to the evaluation of propulsion unit that can generate steady thrust for supply power. It is defined as

$$I_{sp} = \frac{\int f dt}{g_o \int \dot{m} dt} = \frac{v}{g_o} \quad (1.1)$$

where f is thrust, \dot{m} is mass flow rate of exhaust, v is velocity of exhaust, g_o is gravitational acceleration at sea level[1]. In this equation, specific impulse indicates that the thrust per unit consumed propellant mass. Propulsion units with unsteady thrust for supply power, which can control the mass flow rate and supply power separately, or cannot control feed required amount of propellant, are evaluated by momentum coupling coefficient. It is defined as

$$C_m = \frac{\int \dot{m} v dt}{E_{supply}} = \frac{mv}{E_{supply}} \quad (1.2)$$

where mv is impulse bit of exhaust, E_{supply} is supply energy. In the other word, momentum coupling coefficient show the quantity of unit supply energy that can varies the motion trajectory.

The detail of the target propulsion unit type in this research will be described later part, it cannot control the consumed mass amount precisely due to the propellant supply principle. Furthermore, this thruster generates momentary thrust and generally evaluated in impulse bit. Therefore, momentum coupling coefficient is applied as basic evaluation item in this thesis.

1.2. Research background

In recent years, the global interest in space development is increased. In particular, with the rapid development of communication technology, it attracts attention of private enterprises in terms of constructing a communication network. For example, OneWeb LLC which is a global communications company in USA plans to connect the globe by approximately 600 low orbital (at 1200 km altitude) satellites in coming ten years [1]. One suitable technology for such demands is the small satellite which is defined as the satellite with a net weight less than 500 kg. The appeal of this type of satellite is the low cost of development and launch. Although available missions are limited compared with the large artificial satellites, the development period and cost can be reduced because the required technical hurdles are relatively low. Thus the cost can reduced by launching with other artificial satellites such as the piggyback satellite [5].

The core technology in the small satellites development is the small propulsion unit that is called the micro-thruster. The requirements of this thruster include the following four elements:

1. Light weight and miniaturization easiness
2. Low consumption of electrical energy (less than several hundred W)
3. Wide thrust range which can correspond from the attitude control to the orbital transition
4. High specific thrust and propulsion efficiency

Normally, a satellites equipped with two types of propulsion units for attitude control and orbital transition separately. However, a small satellite cannot load multiple propulsion units due to the weight and volume limits. Therefore, the propulsion unit must achieve both functions as slated in (3). The final requirement presented in (4) is an indispensable condition for effective acceleration due to the reducing power source weight and propellant weight[6].

The propulsion unit of a space craft can be implemented by either electric and chemical types. The chemical propulsion unit can generate a strong thrust, but its specific thrust is low. Therefore, it is normally applied in the short period mission such as launch vehicle. But the electric propulsion unit is a high specific thrust even with a tiny thrust which is suitable as a micro-thruster. The specific thrust of the electric propulsion unit can exceed 1000 s, while the specific thrust of the cold gas jet that has been used as an attitude control propulsion unit for satellite is approximately several 10 s. For example, the gas jet thruster of PROCYON which is an ultra-small satellite for deep space exploration

(developed by Intelligent Space System Laboratory, The University of Tokyo) can generate only 24 s specific thrust [7]. Thus the electric propulsion shows great advantages on its thrust performance. However, the electric propulsion system must be required scale down. But the thruster performance is also going down as the size scaled down. For example, the arc jet thruster can work with low power such as less than 100 W. But if the output power is 400 W or less, thrust performance decrease sharply [8].

“Pulsed Plasma Thruster (PPT)” is one of the most promising candidate electric thrusters as micro-thruster with less than 100 W power consumption. In an amount of previous works, PPTs normally use solid propellants and generate plasma by the propellant sublimation by pulsed arc discharge. And the plasma is then accelerated electromagnetically or electrothermally. The solid propellant PPT is called Ablative Pulsed Plasma Thruster (APPT) since the solid propellant in it is supplied to the discharge room by ablation process ignited by the arc discharge. In addition, by the simple structure of a APPT, is easy to be minimized and scaled down in size and weight.

However, there are still a number of limitations a real-word APPT operation. One primary defect is their low efficiency (typically less than 10 % [9]. Poor propellant utilization due to the generation of heavy neutral mass is the major reason identified for this low efficiency. The major mechanism of generating heavy neutral mass is the Late Time Ablation (LTA). LTA is the process of the solid propellant sublimation from the consumed surface after plasma generation, which is caused by the radiation of generated plasma [11]. Since the gas is neutral, which is non-conductive, it cannot promote thrust because it cannot be accelerated by the electromagnetic force. The gas is then ejected due to the tiny force caused by the increased enthalpy. The primary limitation of LTA is that the almost component of consumed mass is that neutral gas. As an example, in the propulsion unit of the Lincoln 12 Experimental Satellite (LES-6), the charge accumulation in the Faraday cup shows that the ionized mass is only approximately 1 μg of the total 10 μg , indicating an extremely low efficiency of the propellant.[12]

The second limitation factor is the contamination of exhausted gases. The typical propellant of the APPT is the Polytetrafluoroethylene (PTFE) as solid propellant based on an amount of previous studies [1]. Since PTFE is a polymer including C_2F_4 as a monomer, PPT exhaust contains atoms and compounds consisting of carbon and fluorine. Since the chemical reactivity of fluorine is strong, the negative effect to solar cells and other optical equipment is considerable[17]. Meanwhile, the chemical reactivity of carbon is relatively weak, but the light transmissions to solar cells and other optical equipment are blocked due to the generated carbon particles. In addition, if the carbon particles absorbed and deposited between the electrodes, it may cause the PPT malfunction due to the short circuit between various electrodes.

The third limitation factor is the uneven consumption of a solid propellant. If APPT is operated for a long period, a solid propellant can be consumed unevenly thus form an irregular surface which also causes malfunction or decreasing efficiency. Furthermore, since a solid propellant usually can not be consumed completely, the extra propellant load is required in APPT which causes increase of weight and size.

1.3. The objective of this research

In this research, we try to find that how much effect can be seen on ablative pulsed plasma thruster performance by changing the solid propellant shape.

The reason of changing propellant shape is as following.

The first one is to reduce the consume propellant mass. Almost propellant mass is consumed and wasted by the heat transfer of radiation from generated plasma to solid propellant surface. The shape of APPT solid propellant is commonly simple form such as rectangle or cylinder. If solid propellant is processed such as making holes for the consumed surface of solid propellant and increasing the entire surface area, the radiation intensity also be reduced by dispersing the radiation energy due to suppress the temperature rise on the solid propellant surface which is the aim of changing shape. Since PPT can be generate only unstable plasma, estimating the accurate radiation amount is difficult. Therefore, in this research, we estimate the consumed mass of processed solid propellant by assuming that radiation is irradiated uniformly to entire surface in hall. In the other words, we assume that the propellant surface area of radiation irradiated is simply expanded. Since that area is expanded, radiation intensity will be decreased and wasted mass is also decreased.

The second reason is to verify the relation of solid propellant shape and impulse bit or consumed mass. If this relation is shown, the ideal shape of solid propellant might exist. To measure the impulse bit, we made thruster stand what can measure the tiny force in μNs order.

However, if the solid propellant surface density is decreased by perforating on consumed propellant surface, the impulse bits generated by PPT are expected to decrease naturally because the supplied propellant mass should be decreased also. If solid propellant is assumed to consumed uniformly, the impulse bit will be reduced according the density of solid propellant surface.

1.4. Pulsed Plasma Thruster

In this section, the propulsion characteristics and principle of the ablation-fed pulsed plasma thruster generally abbreviated as PPT is reviewed. PPT is a one of the non-stationary operation electromagnetic acceleration type electric thruster for satellites. Of all the various electric propulsion concepts, because of its system simplicity, the APPT was the first to realize acceptance for propulsion unit on space missions. Decades later, the demand of PPT was followed by the other type electrical propulsion unit such as the xenon ion engine, the stationary plasma thruster (SPT), expanded hydrazine thruster, and the arc jet thruster. On the other hand, in contrast with a moment operation propulsion unit as the PPT, these steady-state propulsions optimized their performance levels after development for a lot of years. In fact, the thrust efficiency of SPT-100, that is one kind of a hall-effect ion thruster, and the xenon ion engine achieved 50 %. However, in spite of a much lower efficiency, the PPT was applied the selection for space craft applications in the 1960s because of the low cost, robustness, simplicity and short development period. Since the PPT placed on thus unique position which is not comparable simply with other thruster, there is considerable opportunity to be mounted to a satellite,

however, in same time, it is facing a lot of improvement, especially efficiency [6].

A lot of types of PPT exist depending on electrode shape or solid propellant supplying method. Figure 1.1 displays one kind of the PPT, which is most traditional type, breech-fed, rectangular electrodes, driven by an LCR (inductance-resistance-capacitance) pulse circuit. Usually polytetrafluoroethylene(PTFE) is applied as a solid propellant bar which is installed into the gap between two electrodes. The principle of PPT is as follows:

1. The main capacitor connected to two electrodes is charged at 1-3 kV in vacuum.
2. An igniter generates small amount of initial plasma due to the sublimation of propellant bar around igniter, triggering a radiation energy of electrical discharge across the exposed surface of the solid propellant bar.
3. The initial plasma is grown up and extended between two electrodes due to the electric energy and fields of charged capacitor.
4. Since the discharging circuit is closed by extended plasma, the charge in capacitor is released and causes main discharge. At that same time, propellant is supplied moreover to discharge chamber by heart transfer from generated plasma.
5. The generated plasma is accelerated by electromagnetic forces due to the self-induced magnetic field from electrodes and pressure forces.
6. Finally, the accelerated propellant is ejected to downstream direction with expanding discharge area, and the propulsion unit obtains a thrust by this reaction.
7. As the propellant is consumed at each discharge, the propellant bar is pushed axially into the discharge chamber with a simple spring mechanism. It contributes to eliminate the complex system such as a propellant tank or feed control device.

A lot of type of the PPT exist such as the “side-fed” type (Figure 1.2) or the coaxial arrangement (Figure 1.3). The side-fed PPT is supplied two propellant bars from lateral of discharge chamber.

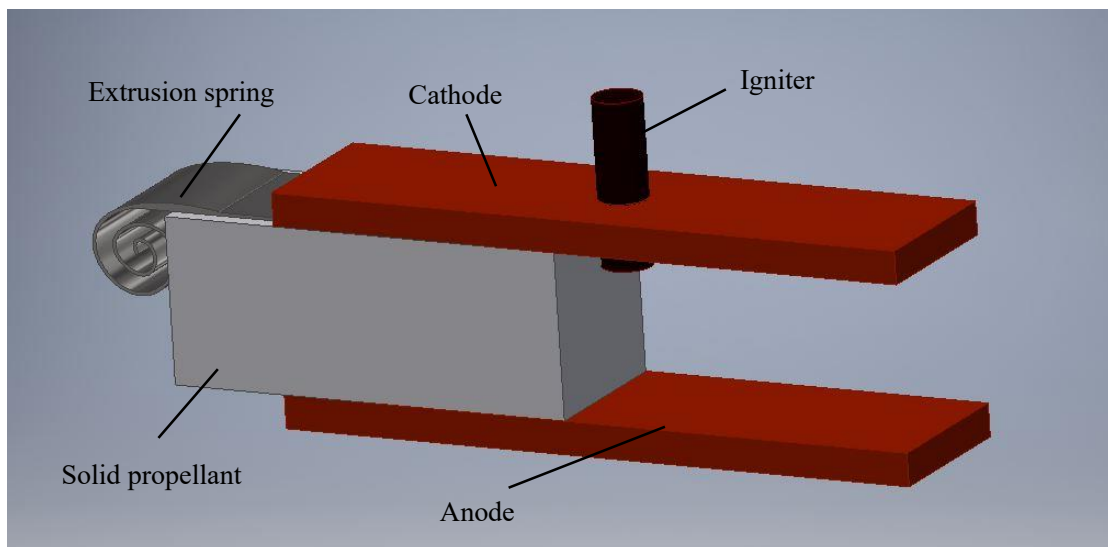


Figure 1.1. Breech fed rectangular type APPT

This type can be applied in rectangular or coaxial electrodes. The coaxial PPT was originally developed as the magnetoplasmadynamic (MPD) thruster, and is member of PPT because of

similarity to PPT in principle.

The systems case for the PPT was considered by Palumbo and Guman based on approximately for 9000 h of PPT operations on LES-6 which is one of the satellite over a 10-year period beginning in 1968, and the character of PPT was reported as a satellite propulsion unit by them as follows:

- 1) Do not need warmup time and standby power.
- 2) No complex mechanism and fail-safe.
- 3) Easy to fit to requirements of mission.
- 4) Usable on stabilization of satellites.
- 5) Advantages of solid propellant: no tank, feedlines, mechanical valves and seals, easy to measure propellant consumption, stability of propellant for temperature or storage period, nontoxic, vacuum compatible, or robustness for variable high “g” loads.
- 6) Compatible with digital logic because of impulse bits.
- 7) Available wide range thrust by operating frequency.
- 8) Satisfying two function of attitude control and orbital transition.
- 9) Capability for variable temperature of environmental.

In addition, the PPT is suitable to the mission requiring a fine position and attitude control of satellites such as formation flying which is required high accuracy of positioning capability. Furthermore, the design with robustness can correspond to immediate operation, even after waiting for a lot of year. These advantages show the reason that the PPT was initially hired on satellite, and development is being continued today.

1.5. PPT Types

As shown in Table 1.1, PPT can be classified to four types depending on this shape and feed mechanism.

Table 1.2. PPT types

Electrode configuration	Rectangular	Coaxial
Feeding method	Breech-fed	Side-fed

The oldest and basic structure of the PPT is the parallel rectangular electrodes with breech-fed type which is driven by a pulse current. This type PPT is represented as the LES-8/9 or EO-1 propulsion unit. The current and self-induced magnetic field for the rectangular electrode configuration are generated primarily transverse to the exhausting direction. The arc discharge attachment regions on the anode and cathode move to downstream along the electrodes with the plasma flow.

The configuration of coaxial type usually hires the conical shape, and typically loads the cylinder solid propellant and two cylinder electrodes in central and downstream as shown in Figure 1.3. The igniter plug in any PPT is usually inserted on the cathode because the negative charge electrons

discharged from igniter are not absorbed to the electrode and irradiated to the solid propellant surface. In the coaxial type, it can be installed either the downstream or the center electrode. The outer cylinder electrode is usually narrow, so that the current inserted at a definite location. Different values of magnetic Reynolds number result in a limited downstream extension depend on current patterns.

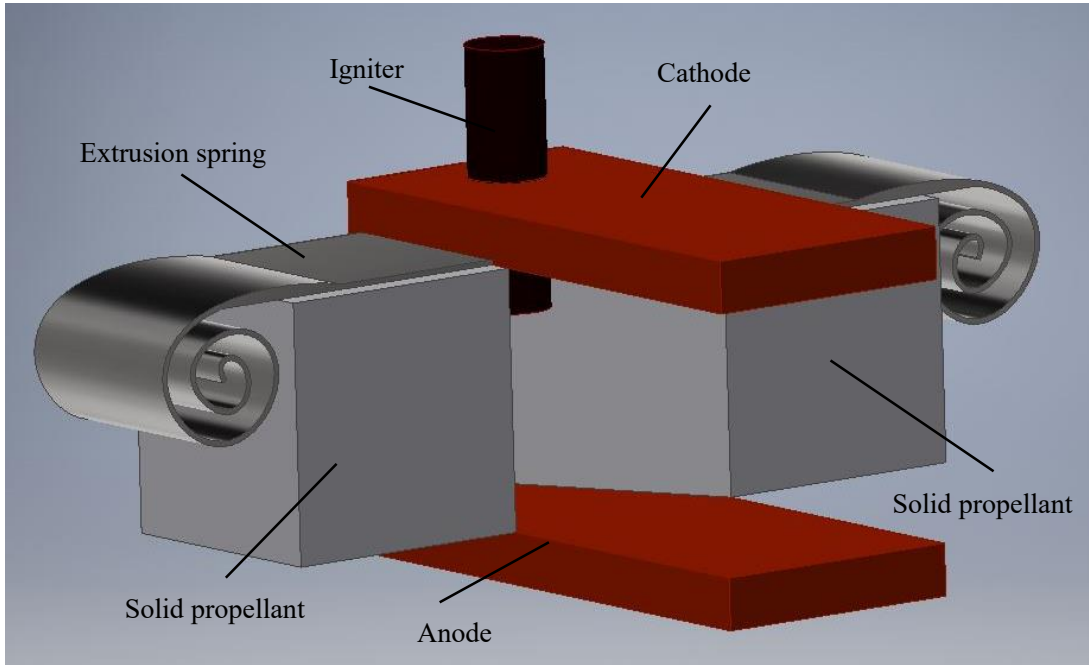


Figure 1.2. Side-fed rectangular type APPT

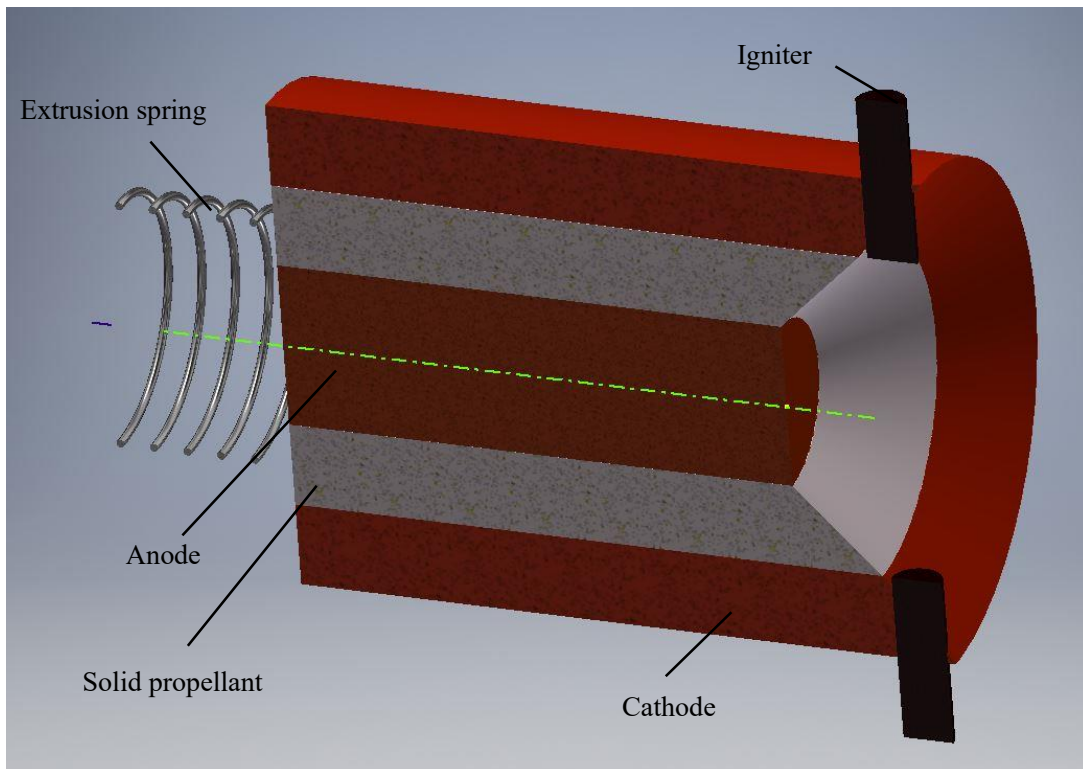


Figure 1.3. Coaxial type PPT

Whether the PPT is breech-fed or side-fed, the operation mode of PPT is the ablation arc or

propagating. These two operating modes are closely similar to deflagration and propagating modes in the PPT with electromagnetic type also using gas injection.

1.6. PPT models

Basically, the PPT obtains thrust by the Lorentz force which is generated between the self-induced magnetic field and the discharge current. That is, this thruster uses that the loop current including plasma receives a force to the out ward direction of the loop due to interact this current and self-induced magnet field.

1.6.1. The model applying LCR circuit

The plasma in PPT is contracted and formed as sheet due to the pinch effect, which is called

“current sheet”. PPT can be modeled as shown in Figure 1.4. The Lorentz force F_{EM} received by current sheet at position x can be obtained by integrating the Lorentz force $\mathbf{j} \times \mathbf{B}$ per unit volume with the volume of the current sheet

$$F_{EM} = \int_x^{x+\delta} \int_0^h \int_0^d \mathbf{j} \times \mathbf{B} dx dy dz \quad (1.3)$$

where j is current density, B is magnetic flux density.

If electromagnetic acceleration wants to be written accurately, there is necessary to

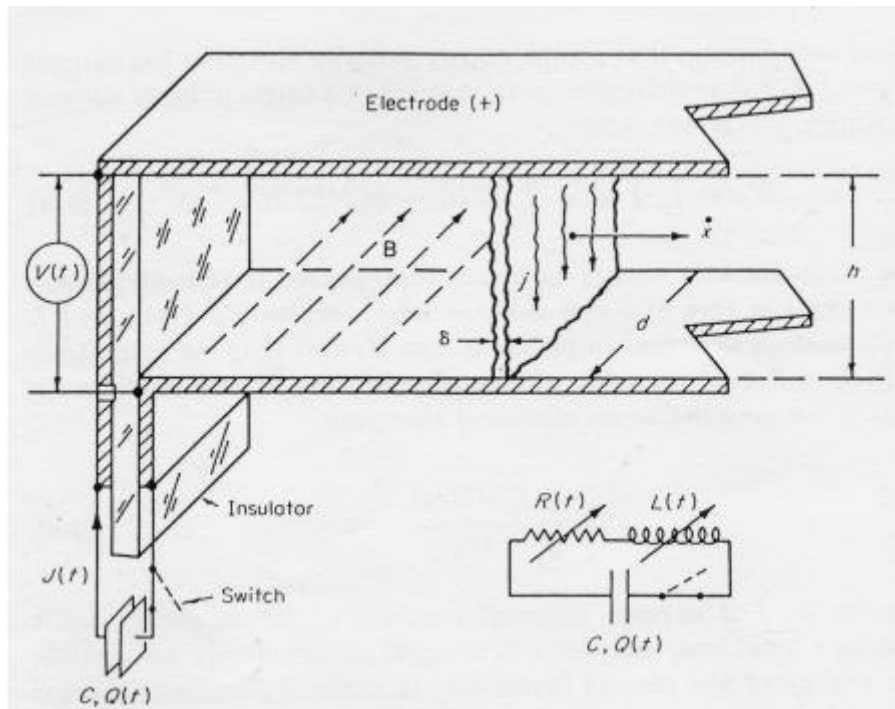


Figure 1.4. The electromagnetic model of PPT[13], $V(t)$: Voltage between electrodes, B : Magnetic flux of self-induced magnet field, $J(t)$: Discharge current, h : Gaps between electrodes, d : Electrode width, δ : Thickness of current sheet

apply MPD theory, however, a formulation or a calculation are extremely complex. Therefore, it come often as an electrical circuit concept by being assumed that a circuit composed of capacitors and electrodes is consisted of lumped constant system. As Figure 1.4, the capacitor with capacitance C is assumed that be charged initial voltage V_0 . when a tiny discharge induced by igniter, the circuit is closed by generated plasma, then, an arc discharge occurs. R_0 is defined the entire circuit resistance immediately after plasma generation and L_0 is inductance. Since the plasma moves to downstream due to the Lorentz force caused by discharge current, the area of the circuit loop increases with time. Therefore, the inductance $L(t)$ at an arbitrary time t is a monotonically increasing function. This rectangular circuit is applied Maxwell law[13]

$$\nabla \times \mathbf{E} = -\frac{\partial \mathbf{B}}{\partial t} \quad (1.4)$$

Area integral along current path

$$\int_S (\nabla \times \mathbf{E}) \cdot d\mathbf{A} = -\int_S \frac{\partial \mathbf{B}}{\partial t} \cdot d\mathbf{A} = -\dot{\phi} \quad (1.5)$$

where S is an area formed by the loop circuit, A is its area vector, ϕ is magnetic flux which is interlinking the area of the loop. Here, the Stokes' theorem is given with Γ that is a loop passing through the edge of area S

$$\oint_{\Gamma} \mathbf{E} \cdot d\mathbf{s} = \int_S (\nabla \times \mathbf{E}) \cdot d\mathbf{A} \quad (1.6)$$

Then, this equation is applied to left side of equation (1.5)

$$\oint_{\Gamma} \mathbf{E} \cdot d\mathbf{s} = -\dot{\phi} \quad (1.7)$$

The relation of any electric field E_a and potential V_a is given as

$$V_a = -\int \mathbf{E}_a \cdot d\mathbf{s} \quad (1.8)$$

Therefore, the equation (1.7) can be shown as follows with the voltage V between electrodes

$$-V + JR = -\dot{\phi} \quad (1.9)$$

Furthermore, it is transformed as

$$\begin{aligned} V &= JR + \dot{\phi} \\ &= JR + \frac{d}{dt}(LJ) \\ &= JR + L\dot{J} + J\dot{L} \end{aligned} \quad (1.10)$$

Since V is also charging voltage of capacitor, this equation can be transformed as

$$JR + L\dot{J} + J\dot{L} + V_0 - \frac{1}{C} \int_0^t J dt = 0 \quad (1.11)$$

In the other hand, the equation of motion of current sheet is given as

$$\frac{d}{dt}(m\dot{x}) = F_{EM} \quad (1.12)$$

FEM is already expressed by equation (1.3), however, it can also be described with the spatial gradient of the electrode inductance

$$F_{EM} = \frac{\nabla L}{2} J^2 \quad (1.13)$$

By the equation (1.11) – equation (1.13), the motion of current sheet can be described. However, the modeling for process of propellant supply should be required because this model does not include it. As the major model, there are “Slug model” and “Snowplow model”. Slug model is assumed that all propellant for one operation is supplied at the same time as the discharge starts. That is, it can be described as $m(t) = m_0$, where m_0 is current sheet at $t = 0$. Snowplow model is the idea that current sheet mass increase due to the sheet absorbing ambient gas while the sheet is going to downstream. In this case, the current sheet mass $m(t)$ is given as

$$m(t) = m_0 + \int_0^t \rho(x) \dot{x} dt \quad (1.14)$$

where $\rho(x)$ is the gas density at position x . If the gas density is constant in discharge channel, above equation can be described as

$$m(x) = m_0 + hd\rho x \quad (1.15)$$

For improving performance of PPT, it is necessary to consider about efficiency relational expression between the initial inductance L_0 and the inductance increase ΔL due to the current sheet moving. By the multiplying both sides of equation (1.10) by current J , the supplied power from capacitor to circuit can be found

$$\begin{aligned} P = \mathbf{JV} &= \mathbf{J}^2 R + L\mathbf{J} \frac{d\mathbf{J}}{dt} + \mathbf{J}^2 \dot{L} \\ &= \mathbf{J}^2 R + \frac{d}{dt} \left(\frac{1}{2} L\mathbf{J}^2 \right) + \frac{1}{2} \dot{L}\mathbf{J}^2 \end{aligned} \quad (1.16)$$

In this equation, the first term is equivalent to Joule heating per unit time, the second term is varying energy over time, the third term shows the consumed power for current sheet transfer, in other word, the power of electromagnetic acceleration. By the integral this P with time, the energy amount W_0 supplied from the capacitor can be expressed as

$$\begin{aligned} W_0 &= \int_0^\tau P dt \\ &= \int_0^\tau \left(\mathbf{J}^2 R + \frac{d}{dt} \left(\frac{1}{2} L\mathbf{J}^2 \right) + \frac{1}{2} \dot{L}\mathbf{J}^2 \right) dt \\ &= \int_0^\tau \left(\mathbf{J}^2 R + \frac{1}{2} \dot{L}\mathbf{J}^2 \right) dt \end{aligned} \quad (1.17)$$

Since \mathbf{J}^2 is in common term of R and $\frac{1}{2}\dot{L}$, \dot{L} is identical dimension of R . The energy ratio η_e of the charged energy in capacitor and consumed energy for electromagnetic acceleration is defined as

$$\eta_e = \frac{1}{2} \frac{\int_0^\tau \mathbf{J}^2 \dot{L} dt}{W_0} \quad (1.18)$$

However, it is assumed that the energy of electromagnetic acceleration gained by propellant is not lost and is completely converted to physical energy. To estimate order of η_e , the current amplitude value J_0 with following condition is applied

- Zero resistance of circuit
- The entire circuit inductance is fixed initial value L_0
- The discharge current is a sine wave with amplitude J_0

The above condition cannot be realized naturally, these are just reference value for estimation of efficiency η_e . In this case, the charged energy W_0 in capacitor equals the charged energy $\frac{1}{2}L_0V_0^2$ in inductor

$$W_0 = \frac{1}{2}L_0v_0^2 \quad (1.19)$$

Equation (1.19) and (1.18) are combined as

$$\eta_e = \frac{\int_0^\tau J^2 \dot{L} dt}{L_0 I_0^2} \quad (1.20)$$

Due to the inductance monotonous increase with time, and resistance R is a finite value, $J < J_0$. Therefore, the efficiency η_e is given by

$$\eta_e = \frac{\int_0^\tau J^2 \dot{L} dt}{L_0 I_0^2} < \frac{\int_0^\tau J_0^2 \dot{L} dt}{J_0^2 L_0} = \frac{\Delta L}{L_0} \quad (1.21)$$

where ΔL equals $\int_0^\tau \dot{L} dt$, which means the increase of inductance amount due to the current sheet moving to downstream. From the above equation, the PPT performance depends on the initial inductance L_0 and the increase of inductance amount ΔL due to the current sheet moving. Since the inductance is known as that it is decided by the shape condition as electrode width, length or gaps, the initial inductance L_0 depends on the shape of circuit and the increase of inductance amount ΔL depends on shape of electrode. This fact indicates that when we design the PPT, we must to care the shape of electrode or feedthrough.

To make it easy, by the applying electric charge Q with assumption that each parameter L and R in the discharge circuit are constant, the following second order linear differential equation is given

$$L_0 \ddot{q} + R_0 \dot{q} + \frac{Q}{C} = 0 \quad (1.22)$$

$$Q(0) = CV_0 \quad (1.23)$$

$$\dot{Q}(0) = -J(0) = 0$$

If the above equation is solved and assigned to following equation, $V(t)$ and $J(t)$ is obtained

$$\mathbf{J} = -\dot{Q} \quad (1.24)$$

$$\mathbf{J} = \frac{Q}{C} \quad (1.25)$$

The analytical solution of equation (1.24) can be classified into the following three types according to value of $CR_0^2/4L_0$ which depends on L , C and R . When $CR_0^2/4L_0 < 1$, it is the inadequate damping waveform, and the waveform of current and voltage are described as

$$V = \frac{V_0}{\omega} \sqrt{\frac{C}{L_0}} \exp\left(-\left(\frac{R}{2L_0}\right)t\right) \sin(\omega t + \delta) \quad (1.26)$$

$$J = \frac{V_0}{L_0\omega} \exp\left(-\left(\frac{R}{2L_0}\right)t\right) \sin(\omega t) \quad (1.27)$$

where ω and δ are

$$\omega = \left(\frac{1}{L_0C} - \frac{R_0^2}{4L_0^2}\right)^{\frac{1}{2}} \quad (1.28)$$

$$\delta = \tan^{-1}\left(\frac{4L_0}{R_0^2C} - 1\right)^{\frac{1}{2}} \quad (1.29)$$

In the case of $CR_0^2/4L_0 = 1$, the waveform is critical damping

$$V = CV_0 \left(1 + \frac{R_0}{2L_0}t\right) \exp\left(-\frac{R_0}{2L_0}t\right) \quad (1.30)$$

$$J = \frac{V_0}{L_0} \exp\left(-\left(\frac{R}{2L_0}\right)t\right) \quad (1.31)$$

In the case of $CR_0^2/4L_0 > 1$, the waveform is overdamping

$$V = \frac{V_0}{\omega'} \sqrt{\frac{C}{L_0}} \exp\left(-\left(\frac{R}{2L_0}\right)t\right) \sinh(\omega't + \delta') \quad (1.32)$$

$$J = \frac{V_0}{L_0\omega'} \exp\left(-\left(\frac{R}{2L_0}\right)t\right) \sinh(\omega't) \quad (1.33)$$

where ω' and δ' are

$$\omega' = \left(\frac{R_0^2}{4L_0^2} - \frac{1}{L_0 C} \right)^{\frac{1}{2}} = i\omega \quad (1.34)$$

$$\delta' = \tanh^{-1} \left(1 - \frac{4L_0}{R_0^2 C} \right)^{\frac{1}{2}} \quad (1.35)$$

In a real PPT, the capacitor inductance or the inductance between electrodes are at least 10 nH, and the capacitance of the capacitor is approximately 100 μ F at most. Therefore, the current or voltage waveform are usually the inadequate damping because of $CR_0^2/4L_0 < 1$. Since L_0 and R_0 are important parameters that affect PPT performance, the equation to find the entire inductance L and the entire resistance R should be derived from discharge current and voltage waveforms. To make it easy, the equation (1.27) can be described as following with the logarithmic decay rate α and angular frequency ω

$$J = J_a \exp(-\alpha t) \sin(\omega t) \quad (1.36)$$

$$\omega = \sqrt{\frac{1}{LC} - \frac{R^2}{4L^2}} \quad (1.37)$$

$$\alpha = \frac{R}{4L} \quad (1.38)$$

The ratio of time t_{peak} at the maximum current and the current after one period is given by

$$\frac{J(t_{\text{peak}})}{J(t_{\text{peak}} + T)} = \frac{J_a \exp(-\alpha t_{\text{peak}})}{J_a \exp(-\alpha t_{\text{peak}} + T)} \quad (1.39)$$

where T is one period shown as $T=2\pi/\omega$. By the applying natural logarithm of both sides of above equation, the logarithm decay ratio is described as

$$\alpha = \frac{\ln \left(\frac{J(t_{\text{peak}})}{J(t_{\text{peak}}+T)} \right)}{T} \quad (1.40)$$

L and R can be expressed by α

$$L = \frac{1}{C(\omega^2 + \alpha^2)} \quad (1.41)$$

$$R = \frac{2\alpha}{C(\omega^2 + \alpha^2)} \quad (1.42)$$

Therefore, L and R can be calculated by assigning each value of the peak current and its time to the equation (1.40) – (1.42). Incidentally, this calculation is possible with the waveform of discharge voltage.

1.6.2. The model applying MHD theory

In this subsection, the relation of the energy of PPT, mass shot and impulse bit is described by the ideal MHD model which is application of MHD theory with quasi-stationary and one dimension. If the PPT discharge is assumed that the discharge type is quasi-steady mode, the discharge is kept at propellant surface. Quasi-steady mode is one of the condition that conductive particles always stay at propellant surface by a sufficient heat transfer from the generated plasma to propellant. Under the quasi-steady condition, the magnetic Reynolds number is less than 1, which means that the generated plasma is frozen on magnetic fields. In addition, if the ratio β of a pressure and a magnetic field pressure is small enough and the gas dynamic effect can be ignored, the condition of magnetic sound velocity can be satisfied because PPT inject to free vacuum. Therefore, following equation at magnetic sound velocity can be described as

$$\mathbf{u}^* = V_A^* = \frac{B^*}{\sqrt{\mu\rho^*}} \quad (1.43)$$

where u is a flow velocity, V_A is a partial Alfvén velocity, ρ is a density and B is a magnetic flux density. “*” means that it is the value at the point of magnetic sound velocity. The magnetic flux density at a propellant surface of the rectangular electrodes channel back side is given by

$$B_0 = \frac{\mu J}{d} \quad (1.44)$$

where J is an entire discharge current, d is a width of an electrode. In addition, if the mass flow rate per unit area on the rectangular cross section as Figure 1.4 is expressed as $\omega = \dot{m}/dh$, the equation of continuity, the physics equation, the energy equation are given by

$$\rho u dh = \dot{m} \quad (1.45)$$

$$\rho u = j B_z \quad (1.46)$$

$$\frac{\dot{m}}{dh} h_0 + \frac{E B_0}{\mu} = \frac{\dot{m}}{dh} \left(h + \frac{u^2}{2} \right) + \frac{E B}{\mu} \quad (1.47)$$

where \dot{m} is a mass flow rate of propellant, E is an electric field strength which is uniform in channel, h is specific enthalpy. Since the gas dynamic pressure can be ignored because of low B , the pressure gradient term is deleted from equation (1.47). If Hall effect is ignored, j is described as follows by ampere's circuital law

$$j = \frac{1}{\mu} \frac{dB_z}{dx} \quad (1.48)$$

In the case with the extended Ohm's law, j is expressed as

$$j = \sigma(E - \mathbf{u} B_z) \quad (1.49)$$

The equation (1.46) and the equation (1.48) are assigned to the equation (1.47)

$$\frac{\dot{m}}{dh} \frac{du}{dx} = -\frac{1}{\mu} B_z \left(\frac{dB_z}{dz} \right) = -\frac{1}{2\mu} ddx B_z^2 \quad (1.50)$$

The integral of the equation (1.46), (1.47), (1.50) from the propellant surface to the point of magnetic sound velocity are described as

$$\rho^* \mathbf{u}^* dh = \dot{m} \quad (1.51)$$

$$\frac{\dot{m}}{dh} \mathbf{u}^* = \frac{1}{2\mu} (B_0^2 - B^{*2}) \quad (1.52)$$

$$\frac{\dot{m}}{dh} h_0 + \frac{E B_0}{\mu} = \frac{\dot{m}}{dh} \left(h^* + \frac{u^{*2}}{2} \right) + \frac{E B^*}{\mu} \quad (1.53)$$

By above equations and the equation (1.43), the magnetic field at magnetic sound velocity point is shown by

$$B^* = \frac{B_0}{\sqrt{3}} \quad (1.54)$$

Furthermore, by above equation and the equation (1.46) and (1.47), the magnetic sound velocity can be given by

$$\mathbf{u}^* = \sqrt{\frac{\Delta h}{\sqrt{3} - 1.5}} \quad (1.55)$$

where Δh equals $h^* - h_0$. If a specific energy for ionization or other somethings is assumed that it equals the enthalpy change Δh of flow, the magnetic sound velocity u^* is constant and proportional to Alfven critical velocity u_{crit} which is given by

$$\mathbf{u}_{\text{crit}} = \sqrt{2\Delta h} = \sqrt{\frac{2eV_i}{M}} \quad (1.56)$$

where M is a mass of propellant molecule accelerated by u_{crit} . By the equation (1.55) and (1.56),

$$\mathbf{u}^* = \frac{\mathbf{u}_{\text{crit}}}{\sqrt{2}} \frac{1}{\sqrt{\sqrt{3} - 1.5}} = 1.47\mathbf{u}_{\text{crit}} \quad (1.57)$$

As shown in equation (1.53), a difference in magnetic pressure from the propellant surface to the point of magnetic sound velocity decides a mass flow ratio per aria unit if u^* is constant. In addition, by assignment equation (1.44) and (1.54) to equation (1.53), the mass flow rate is depended on the square of current J and channel width. In other words, the mass flow rate $\dot{m} \approx \Delta m$ is proportional to the square of discharge current. Therefore, PPT has a tendency as follows

$$\dot{m} \propto F \propto J^2 \quad (1.58)$$

The thrust by electromagnetic acceleration is described with same form of equation (1.53) as

$$\frac{\dot{m}}{dh} \mathbf{U}_e = \frac{1}{2\mu} \mathbf{B}_0^2 \quad (1.59)$$

where \mathbf{U}_e is an exhaust velocity. The thrust \mathbf{F}_{EM} by electromagnetic acceleration is

$$\begin{aligned} \mathbf{F}_{\text{EM}} &= \dot{m}\mathbf{U}_e \\ &= dh \frac{1}{2\mu} \mathbf{B}_0^2 \end{aligned} \quad (1.60)$$

Since the magnetic flux density at propellant surface is expressed as $\mathbf{B}_0 = \mu \mathbf{J}/d$,

$$F_{EM} = dh \frac{1}{2\mu} \left(\frac{\mu J}{d} \right)^2 \quad (1.61)$$

$$= \frac{\mu j^2 h}{2 d} \quad (1.62)$$

By the integration of above equation over time t , impulse bit I_{bit} is given by

$$I_{bit} = \frac{\mu h}{2d} \int_0^T J^2 dt \quad (1.63)$$

1.6.3. The model applying electrothermal acceleration

Guman et al derived the thrust by electorthermal acceleration with assumption that the generated gas is expanded to vacuum when the energy E_0 is supplied to the propellant gas of volume V due to the discharge[5]. In addition, following conditions are applied

- Initial temperature is sufficiently lower than final one.
- Unsteady pressure wave propagates rapidly.
- Average flow velocity is sound velocity.
- Gas expansion is adiabatic.
- Cross section area is constant during flowing.

Therefore, the impulse bit by electrothermal acceleration can be given by

$$I_{bit,ET} = \left[\frac{8(\gamma - 1)}{\gamma^2(\gamma + 1)} \Delta m E_0 \right]^{\frac{1}{2}} \quad (2.62)$$

where γ is a specific heat ratio.

Chapter 2: Experimental equipment

In this chapter, experimental equipment and its principle will be explained. The experimental system is constructed by several part such as APPT power source, igniter control device, vacuum exhaust system, thrust measuring system. Since PPT generates momentum force (unsteady force), PPT is generally evaluated with impulse bit. Therefore, the basic evaluation is carried out with impulse bit and its consumed energy and propellant mass.

2.1. Experiment system

The operating system is shown in Figure 2.1. The order from PPT operation to measurement various parameters are in the following:

1. Capacitor for main discharge is charged from 500 to 1000 V by VC power source.
2. Start measurement by impulse bit measurement device and set the current and voltage measurements to the trigger standby state.
3. The signal generator sends a 60 Hz pulse signal to the igniter module in response to an instruction from PC.
4. PPT operates and releases plasma by small discharge of igniter.
5. The oscilloscope records the discharge current and voltage waveform from Rogowski coil and high voltage measurement probe triggered by itself.
6. The exhaust gas collector of the impulse bit measurement device receives the exhaust gas from the PPT, and the impulse bit data is output as displacement value measured by the laser displacement detector.
7. Wait until the oscillation of the impulse bit measuring instrument has settled and measurement is available again.
8. Repeat from 1 to 7

The thrust of PPT must be measured several times at once because solid propellant ablation is not always the same at each work. In other words, the impulse bit measurement must be performed statistically. Furthermore, the state of solid propellant surface will be changed, so thrust must be measured once every several hundred times operation. The capacitor is charged at 100 mA and is completed in approximately 10 seconds at the maximum. Therefore, the pulse signal is set to transmit according to the charging time, and PPT can be operated automatically. At sometimes, PPT may not work due to igniter malfunction or small plasma production failure even if a signal is sent. Since current and voltage are no change when PPT does not operate, the

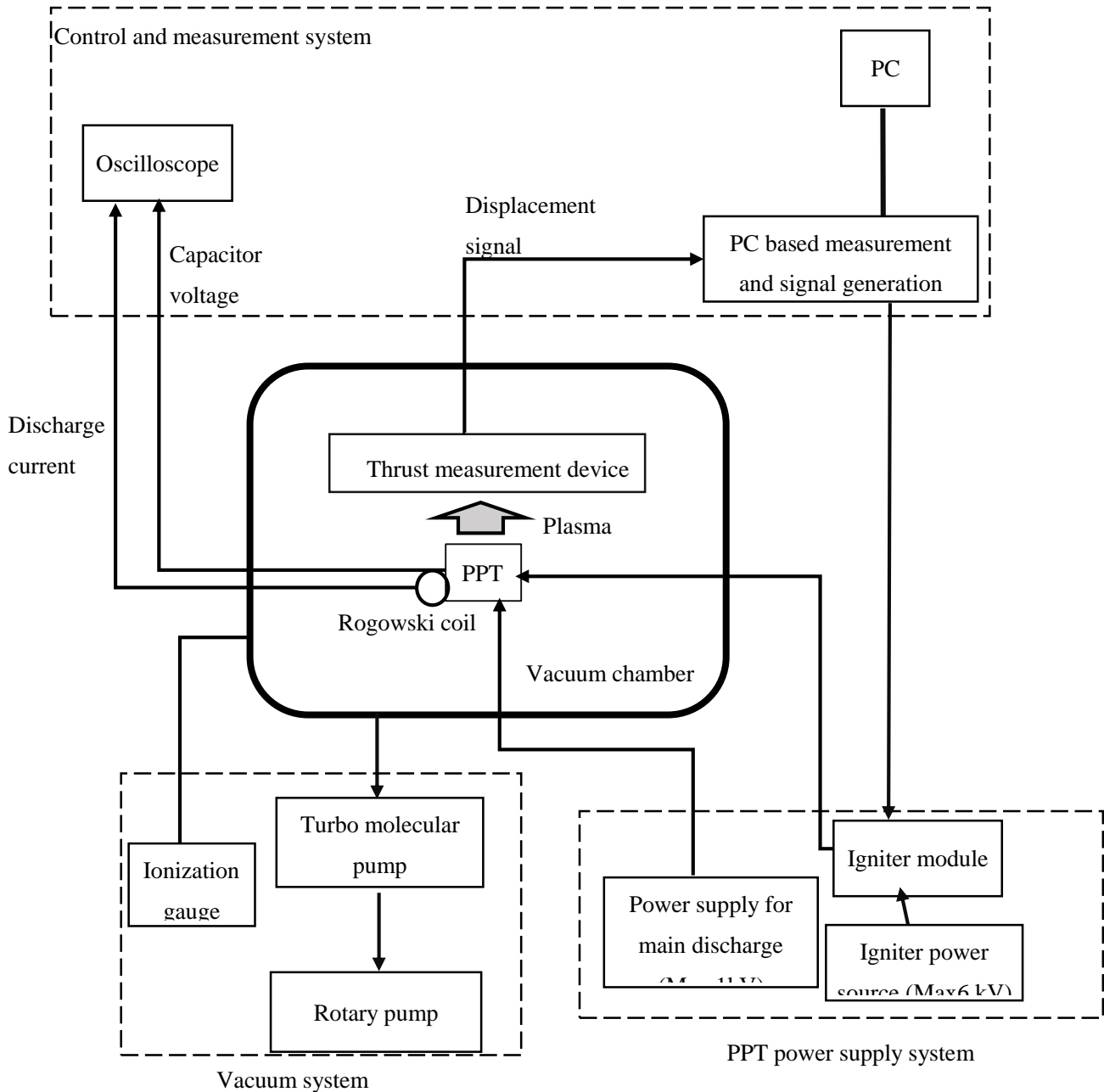


Figure 2.1. Schematic of entire experimental system

oscilloscope is set to save the data when the current trigger is detected, and the number of operations is counted by the number of recorded data.

2.2. Measurement and control equipment

The discharge period is expected that it is extremely short from approximately several tens microseconds to few microseconds. Therefore, the current and voltage waveform measurement equipment is required high resolution. On the other hand, due to the

principle of thrust measurement equipment, the measurement is for several seconds order. Since measurement period of waveform and thrust are much difference, these systems is required to divide.

PPT control is simple because there is only igniter control. That is, it is enough to prepare only the signal generator.

2.2.1. Impulse bit signal receiver and igniter signal generator

The PC-based measurement instrument (WE 500) is adopted to receive thrust data from the thrust measurement device and to transmit s igniter signal. This instrument can transmit or receive various signals by exchanging modules. However, since it is not installed some interface such as monitor, it is necessary to connect to a PC for waveform monitoring and signal transmission.

The signal for igniter is set 60 Hz pulse waveform, as its detail will be explained later, this frequency is decided due to the igniter power source is 60 Hz alternating current. The reason of pulse waveform is that the signal receiver of igniter module is relay circuit, so control with a digital signal is preferable. Duty ratio is 50 %. This signal is transmitted to igniter module between 0.1 Hz and 1 Hz depend on PPT settings.

The thrust information is output as voltage in the range -10 to 10 from thrust measurement device. The output data draws a damped oscillation waveform from 1 to 0.8 Hz. After about 10 seconds from the PPT operation, the damping is completed and the next thrust measurement is standby state.

By the similar frequency of signal transmitting and data receiving, these can be performed on the same device.

2.2.2. Rogowski coil

The maximum discharge current is estimated approximately 21 kA if it is assumed that current is constant and discharge period is 5 μ s. As a method of measuring such a high current waveform, small resistance at $10^{-3} \Omega$ is often inserted into the target circuit. However, inserting resistance causes to decrease PPT performance due to increase inductance or resistance in discharge circuit. That is, this method cannot be hired to this experiment.

In this research, Rogowski coil is applied to measure current because this instrument has some advantages for this experiment as follows:

- Almost no influence on the target circuit due to the non-contact measurement.

- It is high frequency responsiveness characteristics and can correspond to currents with high peak values.
- Easy to downsize and measurable even small circuit such as PPT discharge circuit.
- By the system separated from the circuit including other measuring instruments, noise and ground interference can be avoided.

As shown in Figure 2.2, Rogowski coil is shaped in which a solenoid coil is wound up, and the target current flows its inside.

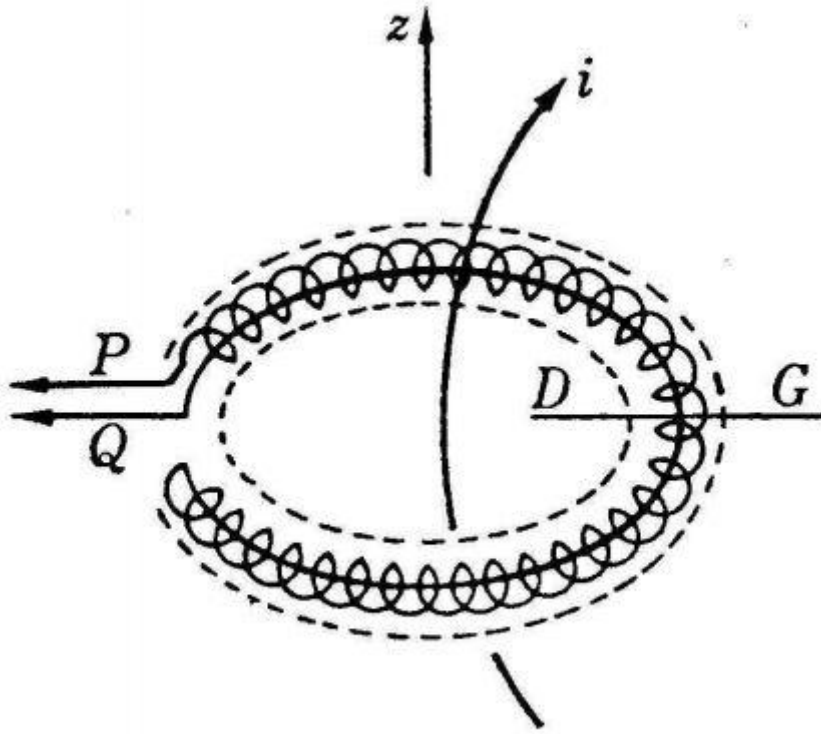


Figure 2.2. Rogowski coil principle [14]

Here, A_{ny} closed curve S surrounding current density vector i is considered. Magnetic flux Φ interlinking solenoid is given by

$$\Phi = \oint_S n\mu H dS + \int_A B_0 dA \quad (3.1)$$

where n is number of turns per unit length of solenoid, a is cross section area of solenoid, μ is permeability, H is magnetic field vector by current i , B_0 is magnetic flux density which is interlinked closed curve area by S , A is area vector formed by closed curve S . As shown in Figure 2.2, if rogowski coil is made as rewinding shape, in other words, if one terminal of the coil is made so as to penetrate the cross section area a , the second term in above equation is canceled and becomes 0. Therefore, equation (3.1) becomes

$$\Phi = \oint_S na\mu HdS \quad (3.2)$$

By Ampere's law

$$\oint_S i = \oint_S HdS \quad (3.3)$$

Therefore,

$$\Phi = \oint_S na\mu HdS = na\mu \oint_S idA \quad (3.4)$$

Faraday's law is given by

$$\Phi = \int_0^\tau e_R(t)dt \quad (3.5)$$

where τ is integration time, $e_R(t)$ is electromotive force between electrodes. If the entire target current is defined as $I = \oint_S i$, the output from Rogowski coil is described as

$$\begin{aligned} I &= \frac{1}{na\mu} \Phi \\ &= \frac{1}{na\mu} \int_0^\tau e_R(t)dt \end{aligned} \quad (3.6)$$

As equation (3.6), the current through into Rogowski coil can be calculated by integration of output voltage. There is a method using integration circuit constructed with resistance and capacitor, however, in this research, current waveform is obtained by analytically.

The Rogowski coil used in this research is made by us as shown in Figure 2.3. In the calibration, this coil is connected to oscilloscope via BMC cable. It is calibrated with 15 kHz alternating current at 20 A, and its sampling interval is 1.0×10^{-7} s. Figure 2.4 shows values that the obtained data just be integrated and multiplied by $1/na\mu$. Peak values are shown in Tabale 2.1. The average of peak current is 13.3 A and the standard deviation is 4.75×10^{-1} A. If original current peak value is assumed at 20 A, the calibration coefficient is 1.509.



Figure 2.3. Rogowski coil appearance

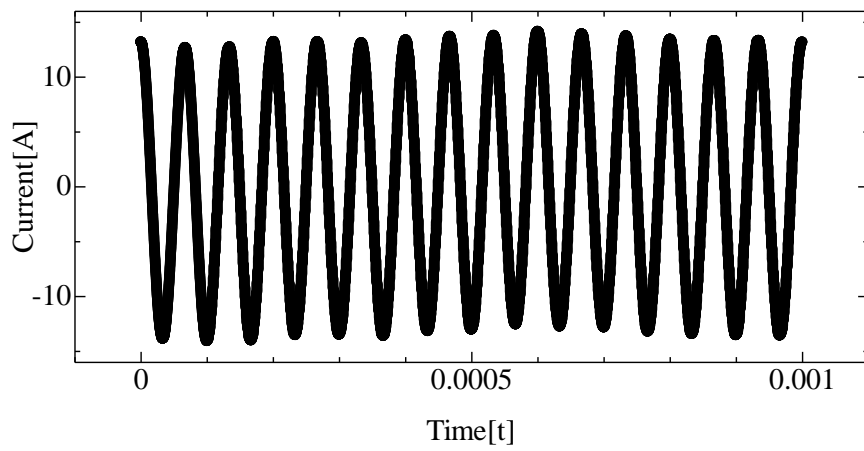


Figure 2.4. Calibration current from Rogowski coil

Table 2.1. Current Peak Values at calibration

Sample number	Current peak value[A]
1	12.7
2	12.7
3	13.2
4	13.2
5	12.7

6	13.1
7	13.4
8	13.7
9	13.8
10	14.1
<hr/>	
Average	13.3

To confirm this calibration coefficient, Table 2.2 shows analyzed current values and its error by multiplication values in Table 2.1 by obtained coefficient. Here, the standard deviation of current peak is 0.72 A and the absolute value average of error is 0.59 A. Since the order of current value of our PPT is estimated as several ten kA, and standard deviation and error average are less than 0.1 % of this order, this Rogowski coil including measuring devices is sufficiently acceptable for current measurement of our PPT.

Table 2.2. Analyzed Current Peak Values and its errors at calibration

Sample number	Current peak value[A]	Error[A]
1	19.12	0.88
2	19.2	0.8
3	19.94	0.06
4	19.91	0.09
5	19.12	0.88
6	19.76	0.24
7	20.18	-0.18
8	20.65	-0.65
9	20.79	-0.79
10	21.34	-1.34
<hr/>		
Average	20	7.1054E-16

Other characteristics of this Rogowski coil are summarized in Table 2.3.

Table 2.3. Characteristics of Rogowski coil

Total turns number N	50
Inside diameter	13.0 mm
Solenoid diameter	7.5 mm
Solenoid length	64.4 mm
Turns number per unit length n	573.9 mm ⁻¹
Cross section area a	44.2 mm ²

$1/na\mu$	$3.14 \times 10^7 \text{ A}^2/\text{Nm}^2$
Calibration factor	0.93

2.2.3. Discharge current and voltage waveform measurement

Discharge period of PPT is approximately several ten microseconds, naturally, a measurement instrument must correspond to this order. Furthermore, the current from Rogowski coil is extremely large, naturally, measurement instrument will be broken if it is connected directly. Therefore, for this measurement, digital phosphor oscilloscope (DPO 4104B-L) produced by Tektronix Co. Ltd is hired, its maximum measurement frequency is 1 GHz. In addition, Rogowski coil is connected via attenuator at -30 dB with 1 W (made by Stack Electronics Co, Ltd.). If the signals is sent via attenuator, the relation between original and detected signal is given by

$$G_p = 10 \log_{10} \left(\frac{V_i}{V_o} \right)^2 \quad (3.7)$$

where G_p is attenuation amount, V_i is attenuated signal, V_o is original signal. Since G_p equals 30 dB,

$$V_o = \sqrt{V_i^2 \times 10^3} \quad (3.8)$$

The obtained signal must be converted with above equation.

2.3. Power supply

The PPT in this research is assumed that charge voltage is from 500 V to 1 kV. In addition, to operate igniter in vacuum requires momentarily high voltage at approximately several kV.

2.3.1. Power supply for PPT

Electric power supply capacity is related with frequency of PPT operation. If a lot of operation is planned, better performance power supply unit should be prepared to avoid experiment period being redundant.

Two power supply unit is prepared in this experiment. One of them is that maximum supply voltage is 500 V and current is 600 mA. Another one is that maximum supply voltage is 1 kV and current is 50 mA. The former will be used in lower voltage experiment at less than 500 V, and the latter will be used higher voltage experiment.

2.3.2. Igniter module

In this experiment case, igniter module including booster circuit is not put into vacuum chamber. Therefore, it must boost in outside and supply to igniter electrode directly in vacuum. Discharge in vacuum is required higher voltage than under atmosphere. Relation of gap d between two electrodes, pressure p between electrodes and start point voltage V_s of discharge is described by Paschen's law as

$$V_s = \frac{pd}{\ln \left[\frac{Apd}{\ln \left(1 + \frac{1}{\gamma} \right)} \right]} \quad (3.9)$$

$$= B \frac{pd}{C + \ln(pd)} \quad (3.10)$$

where γ is average of emitted secondary electrons from cathode surface due to the impact by one positive ion, A and B are decided by relational expression given by

$$\alpha = pA \exp \left[- \frac{B}{\frac{E}{p}} \right] \quad (3.11)$$

where α is impact ionization coefficient, E is electric field. By the equation (3.10), V_s is convex function which include one minimum value. Term of pd should be extremely small value, because pressure p is expressed vacuum pressure as space, which is 10^{-5} torr class. In the actual case, Paschen's law cannot be established at less than that pressure. Therefore, estimated discharge start value by above expressions is just a guide, so exact value is needed to find by experimentally. According to past experiment, the record of discharge at 3 kV was reported. That is, igniter module is made that can generate from 3 kV to 6 kV.

The schematic of igniter module circuit is shown in Figure 2.5. The output voltage can be adjusted by variable autotransformer from 0 V to 100 V. Its operation is controlled by switching relay circuit. The output voltage from variable autotransformer is boosted by voltage converter that convert ratio is 1:60. Therefore, this module can supply from 0 kV to 6 kV.

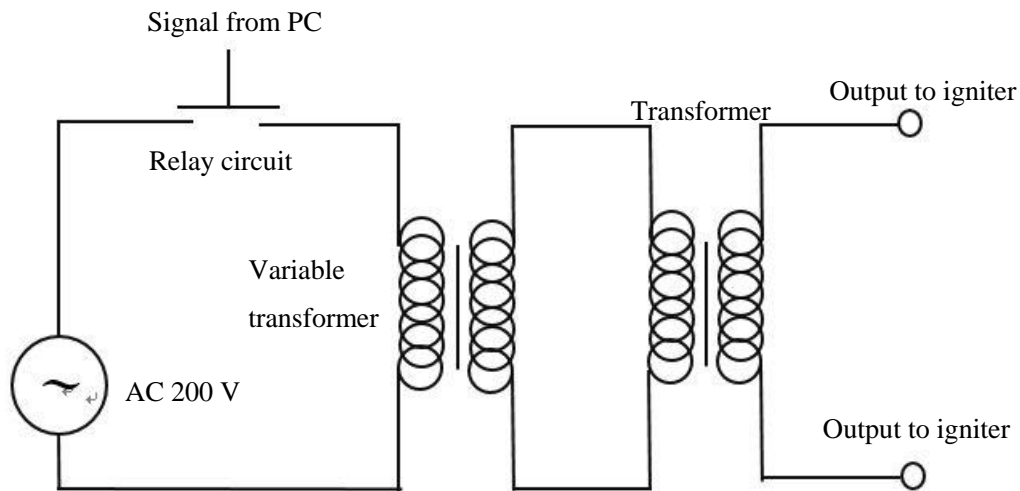


Figure 2.5. Schematic of igniter module

2.4.

Thrust measuring system

The possible thrust of PPT is extremely feeble and momentary. Thus, the special measurement equipment which called “Thruster Stand” exists for electric propulsion unit.

2.4.1 Thruster stand

Thruster stand is usually pendulum construction measurement equipment including spring-mass-damper system. Since thrust is amplified by pendulum construction, tiny power measurement is enabled. If a propulsion unit is independent, it can be measured directly with mounting condition on this equipment. However, the PPT of this experiment cannot be applied this method because it must be connected to outside devices of the system and a cable tension or mass interfere to detected value. For this reason, this

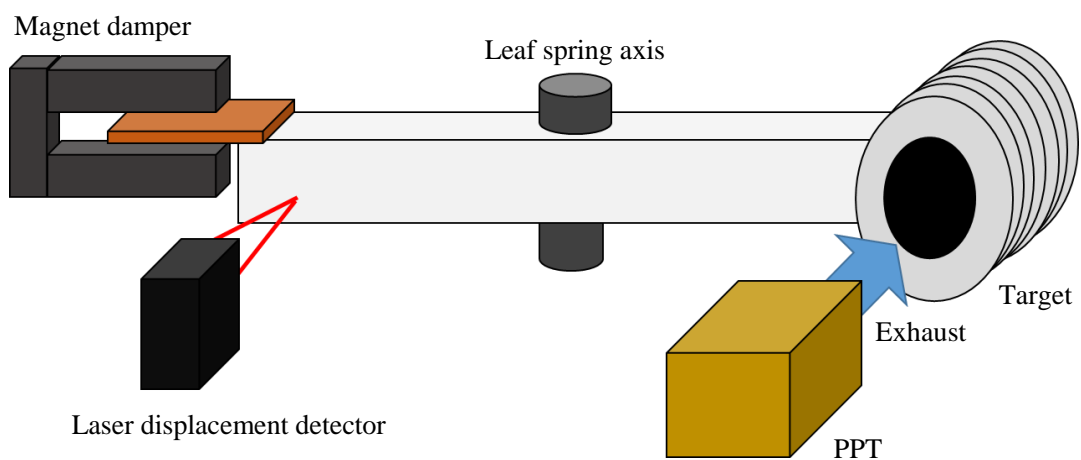


Figure 2.6. Thruster stand principle

experiment is hired measurement method that thrust is measured by receiving exhaust from PPT.

As shown in Figure 2.6, this equipment is constructed of 4 part which is exhaust collector (called target), leaf spring axis, magnetic damper and laser displacement detector. When PPT is operated, particles such as plasma or neutral gas is ejected and impact target. Then, thruster stand begins swinging periodically with the maximum displacement at the balance point with reaction force of leaf spring. Oscillation is damped by magnetic damper, and its waveform is monitored by laser displacement detector. PPT thrust is evaluated by impulse bit, and it is proportional to maximum amplitude of this waveform [15][16]. Therefore, the maximum displacement is recorded.

The target is a cylindrical shape with a lot of slit on the side, and its bottom is a conical shape. The reason of this shape is to prevent error caused by reflected particle between target and PPT by changing direction particles motion in the radial direction. This target is made of 3D-printed high heat resistance resin.

2.4.2 Calibration

The performance of PPT is generally evaluated with impulse bit due to the pulse operation. Therefore, in this experiment, impulse bit by PPT should be converted and obtained directly from displacement data, and calibration coefficient must be able to convert these two elements. As shown in Figure 2.7, calibration is carried out by hummer hitting the target side shaft of thruster stand actually and giving impact. The force of this impact is measured by force transducer which is attached on the tip of hummer. The hummer is pendulum shape as shown in Figure 2.8, and it is pulled and swung by human hand. The impulse bit of hummer impact is calculated by integration of measured force by sample interval time. The waveform of obtained displacement data describes damped oscillation because thruster stand is damped oscillation system including mass, spring and damper. Since the maximum amplitude of this oscillation and calculated impulse bit by hummer are proportional, thruster stand is calibrated by taking these two values multiple times and comparing them. The relational expression of impulse bit I and maximum amplitude A_{max} is given by

$$I = \frac{l_{cal}}{l_t} \frac{I_f}{A_{cal}} A_{max} \quad (3.12)$$

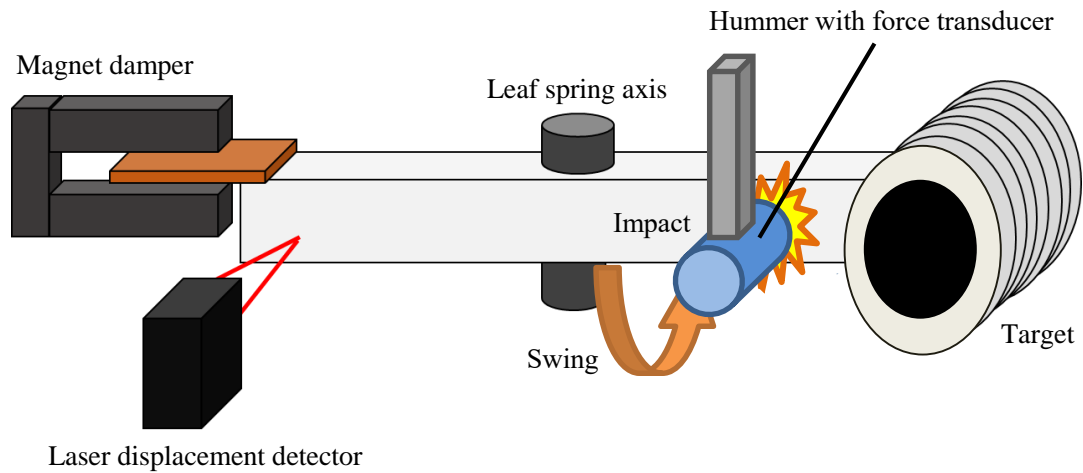


Figure 2.7. Thruster stand calibration method

where l_{cal} is the length of force transducer impact point from leaf spring axis, l_t is the length of target from leaf spring axis, I_f is impulse bit by the calibrator, A_{cal} is maximum amplitude by the calibrator. Here, I_f / A_{cal} is given by least-square method

$$\frac{I_f}{A_{cal}} = \frac{\sum_i A_{cal,i} l_{cal,i}}{\sum_i A_{cal,i}^2} \quad (3.13)$$

Calibration is performed before and after each measurement because target mass probably be changed by contamination of ejected propellant. The force transducer is LVS-500GA made by Kyowa Electronic Instruments Co., Ltd. Its measurable maximum force is 5 N and its error is plus or minus 0.5 %. Therefore, it is guaranteed up to 0.05 N order. If discharge time is assumed to be 10 μ s, measurable impulse bit order is 0.5 μ Ns and it can satisfy the requirement of measurement for PPT impulse bit. One of the example data

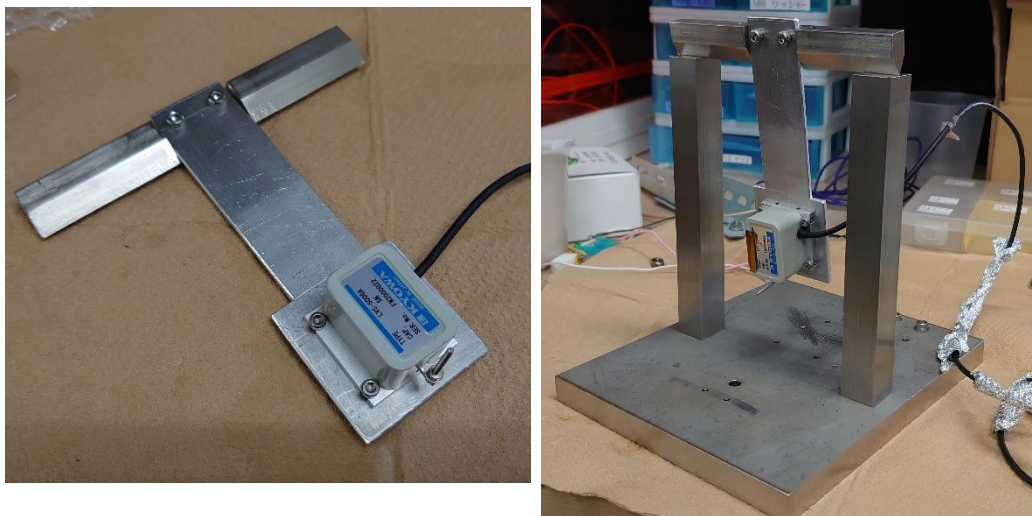


Figure 2.8. Pendulum type Calibration hummer

is shown in Figure 2.7 and 2.8. For Figure 2.7, the force transducer signal describes the oscillation waveform. Since it is considered that the tip of the force transducer vibrates after the collision, the first peak of this waveform should actually be analyzed as impulse. The correlation of this calibration is shown in Figure 2.9. Since there is high correlation which R-square value is 0.9941, the linearity of the output of the thruster stand and the impulse bit should not be a problem.

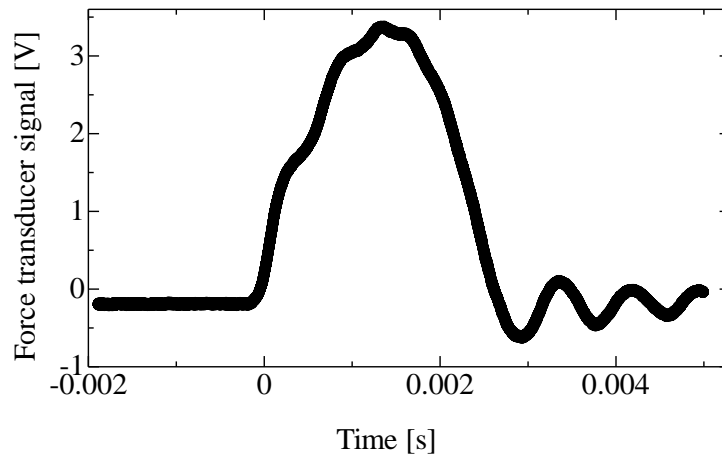


Figure 2.9. Example of calibration data of force

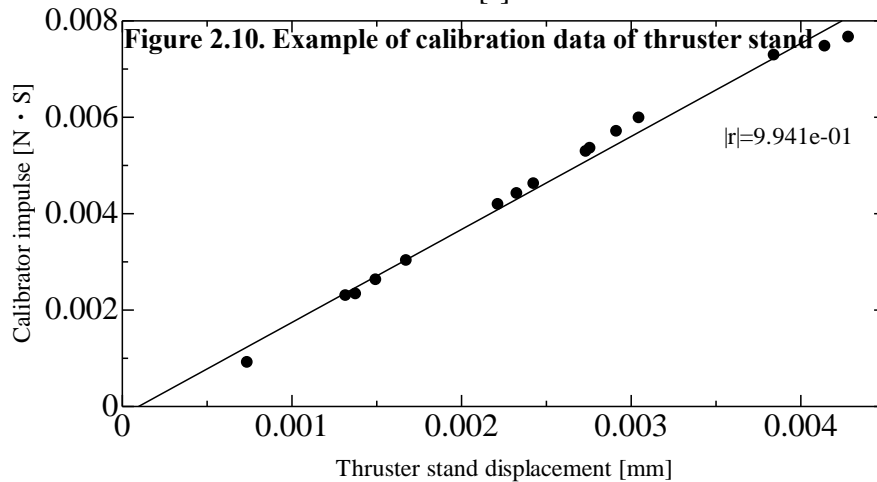
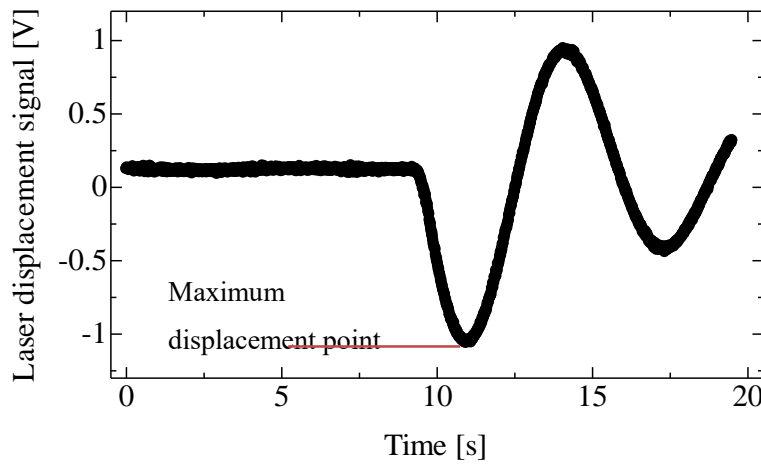


Figure 2.11. Example of calibration line

2.5. Vacuum system

As shown in schematic in Figure 2.10, vacuum system is consisted of a vacuum chamber, a rotary pump, a turbo molecular pump, valves and vacuum gages (Pirani gauge, ionization vacuum gauge). This vacuum chamber is evacuated by a rotary pump and a turbo molecular pump connected in series. The vacuum chamber is installed round and rectangular windows on the side and one round window on the back side. The appearance of vacuum chamber is shown in Figure 2.11. The minimum vacuum pressure is 1.0×10^{-5} torr. Pirani gauge is used in the range of 0.1 to 760 torr, and ionization vacuum gauge is used at less than 10.0×10^{-3} . Experiment is performed at 1.0×10^{-5} to 5.0×10^{-5} which is a high vacuum zone.

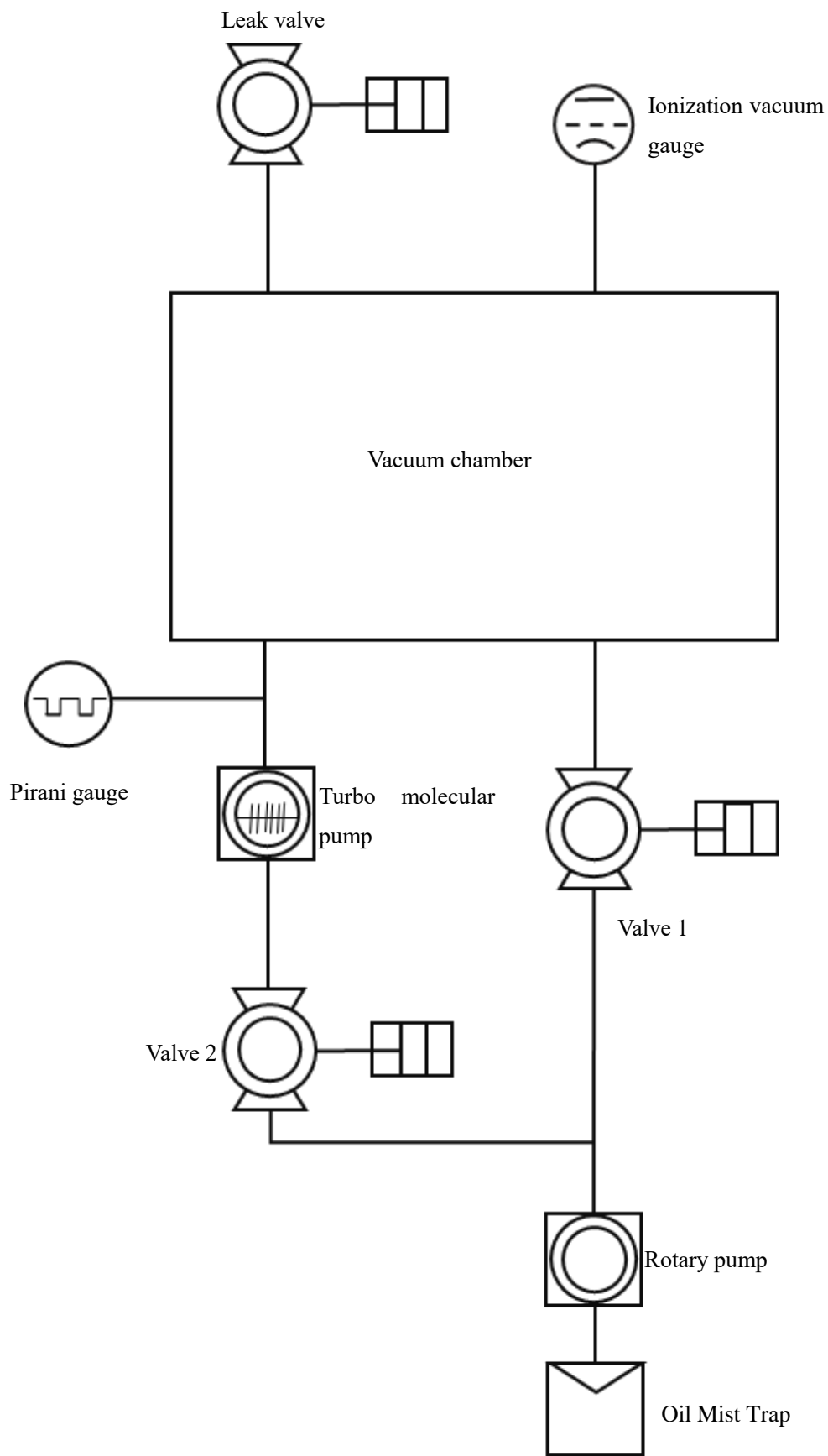


Figure 2.12. Schematic of vacuum system

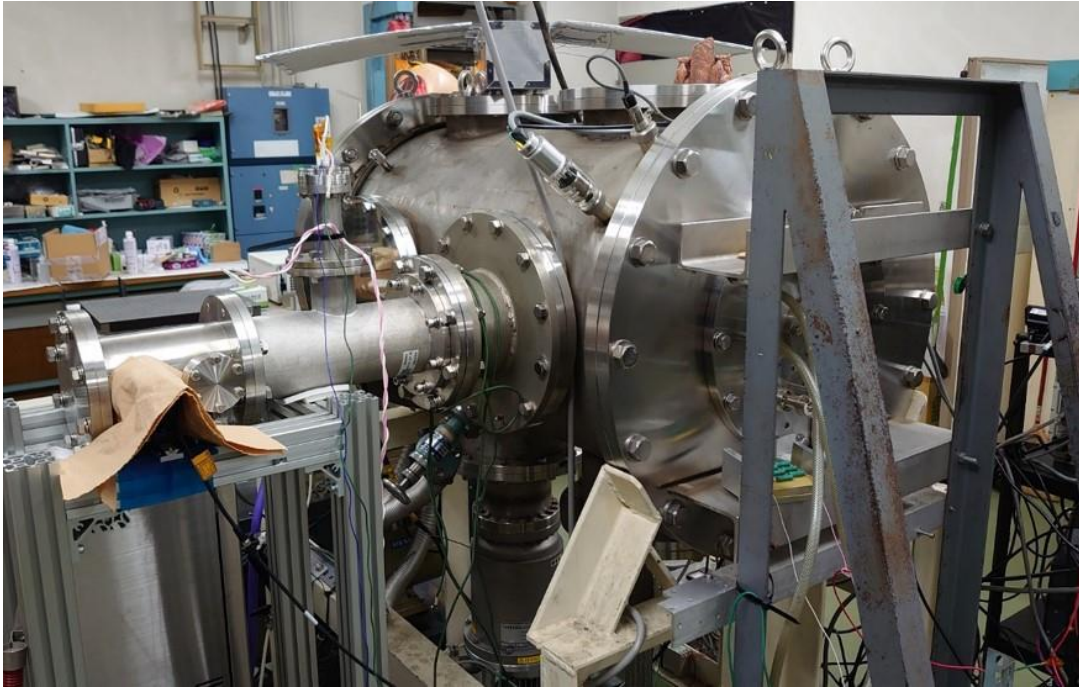


Figure 2.13. Appearance of vacuum chamber

2.6. High speed camera (FASTCAM SA-Z)

To observe plasma behavior, high speed camera (FASTCAM SA-Z: PHOTRON LIMITED Co., Ltd., Figure 2.12) is installed at vacuum chamber aside. Shooting conditions are that the resolution is 120×74 pixels and shooting speed is 504000 fps.



©PHOTRON LIMITED Co., Ltd.

Figure 2.14 FASTCAM SA-Z: PHOTRON LIMITED Co., Ltd.

Chapter 3: Perforated Solid Propellant

Verification

Originally, a propulsion unit for an artificial satellite generally mounts propellant without any gaps in order to effectively use its small mounting space. Therefore, it is natural that the solid propellant for PPT is a simple shape such as rectangular parallelepiped or cylinder. However, since the performance changes depending on the shape of the PPT, the possibility that the performance changes depending on the solid fuel shape of the PPT is also estimated. In this experiment, a new approach to the PPT performance production was carried out.

In this experiment, the thrust and consumed mass are measured and compared with normal solid propellant and perforated solid propellant. Both propellants are respectively tested with two different charging voltages at 500 V, 750 V and 1000 V.

3.1. Laboratory PPT

The appearance of experimental PPT for this work is shown in Figure3.1. This unit is a breech-fed electromagnetic acceleration type PPT with rectangular parallel electrodes. Since PPT is put into vacuum, film capacitor is installed. As shown in circuit diagram (Figure3.2) the capacitor capacity C is 420 μF . Its rated voltage is 1100 V. The gap between electrodes is 15 mm and its width is 10 mm, and its thickness is 2 mm. In addition, this PPT is hired flaring tongue shape electrode, which is reported that yielded an increase in thrust efficiency by nearly 35 % and in exhaust velocity of nearly 20 % [19][20]. The length of this discharge chamber is 20 mm up to the bent part and 20 mm where flaring part. The angle of flaring is 30 degrees. In order to prevent the influence of contamination, electrodes are polished after every experiment to remove the attached carbon. The igniter is biaxial and hired a combination of tungsten and tritungsten at the discharge terminal part, and the thickness is 0.5 mm for tungsten and 0.1 mm for tritungsten. The distance

between igniter tips is approximately 0.5 mm. Installing position is 1 mm from the solid propellant. The solid propellant material is PTFE.

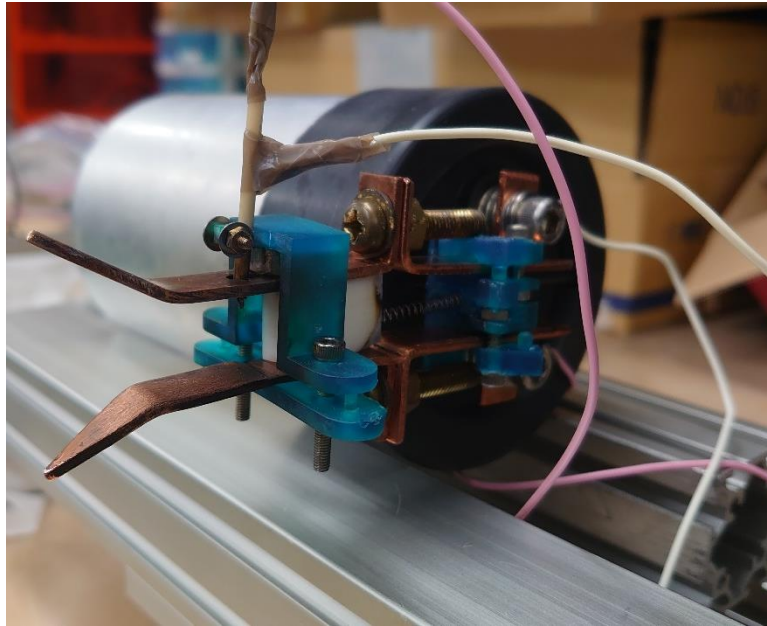


Figure 3.1. Laboratory PPT for perforated solid propellant

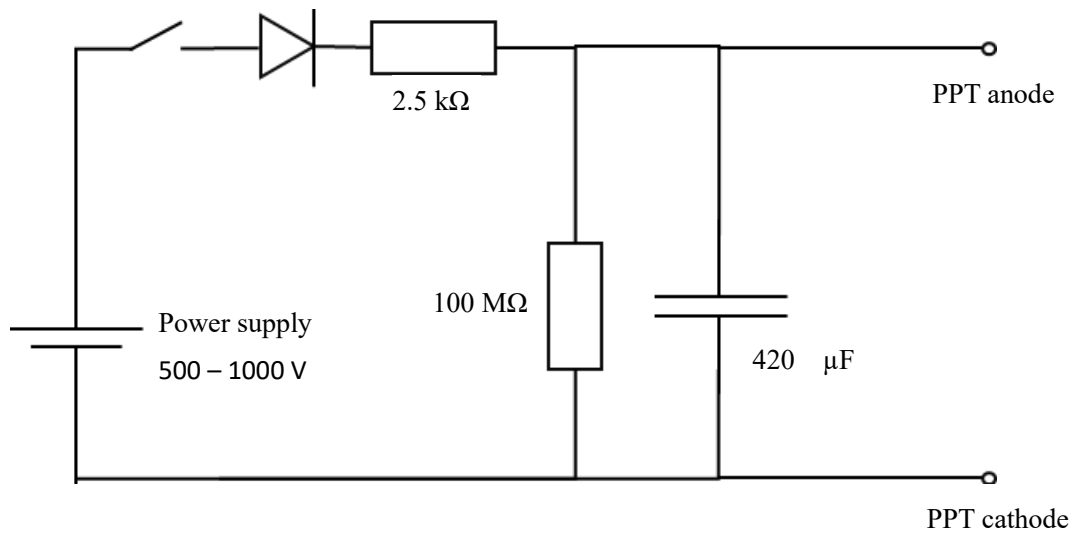


Figure 3.2. PPT circuit diagram

3.2. Normal shape solid propellant test

3.2.1 Normal shape PTFE solid propellant experiment

A large number of propellant types have been evaluated in the hopes of finding improvements over PTFE. The evaluations are usually performed by measuring thrust performance, and by examining the posttest condition of the ablated surface. For example,

the other propellants showed variations in I_{sp} from 947 s (Kel-F) to 2410 s (polyethylene) with PTFE at 1085 s in a breech-fed configuration [21]. As in this example, there are some higher efficient as solid propellant which does not include contamination materials such as fluorine. Nevertheless, the reason why PTFE is selected as PPT solid propellant is its stability for heat. From the previous example, the melting point of polyethylene is from 120 to 140 degree, however, PTFE is 327 degrees. This characteristic is effective to prevent LTA. In addition, it is also an advantage that the stability of the propellant is maintained during continuous operation. Due to those reasons, PTFE was applied as solid propellant in this experiment.

As shown in the Figure3.3, the consumption surface shape of normal shape solid propellant is 15 mm in height and 10 mm in width. The area of consumption surface is 150 mm^2 . After the propellant bar is cleaned by an ultrasonic cleaner, its mass is measured by electronic analytical scale. After experiment, propellant bar is removed and measured

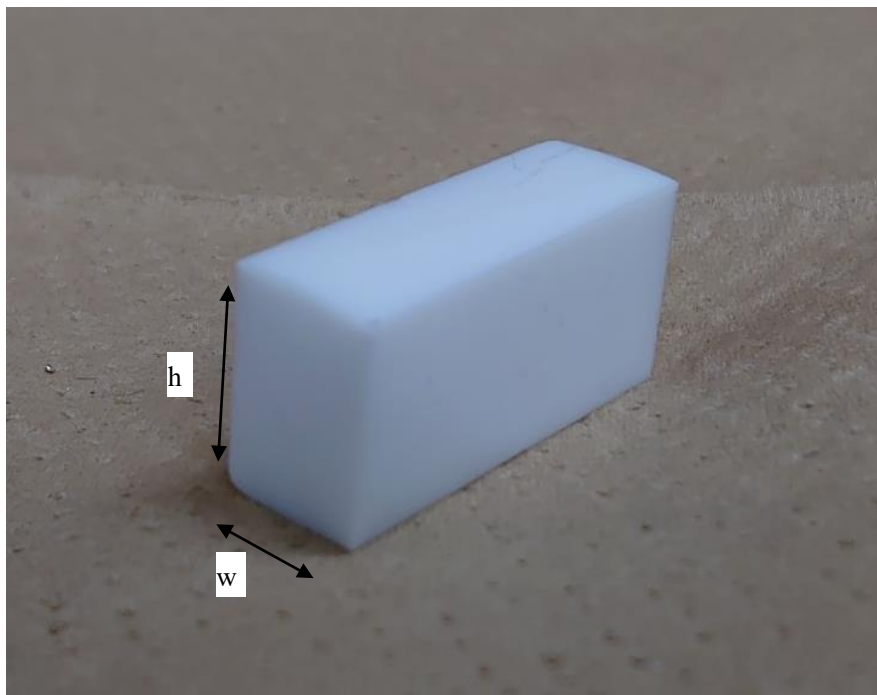


Figure 3.3. Normal shape PTFE solid propellant, $h = 15 \text{ mm}$, $w = 10 \text{ mm}$

directly its mass again. The consumed mass is evaluated by dividing the measured consumed mass by the number of operations.

Figure 3.4 and 3.5 shows the preparation state of the experiment. PPT is fixed with its tip inserted approximately 30 mm into the thruster stand target that is stationary state. Usually, after the solid propellant is sublimated and ionized, it is formed a current sheet due to a pinch effect by electric current, and is ejected by Lorentz force. However, a part of plasma is ejected without a Lorentz force from the side of the discharge chamber due to volume expansion when be sublimated. Since these particles contribute to thrust even though they are minute, they must be collected by the target as much as possible. In

addition, the same applies to neutral gas which is generated due to the LTA after the plasma is exhausted. The Rogowski coil is attached to the cathode (upper side) as Figure 3.4. The current in the cathode is measured by it. The Rogowski coil surface is elaborately insulated to prevent discharge through the coil. The voltage is measured between capacitor terminals by high voltage probe.

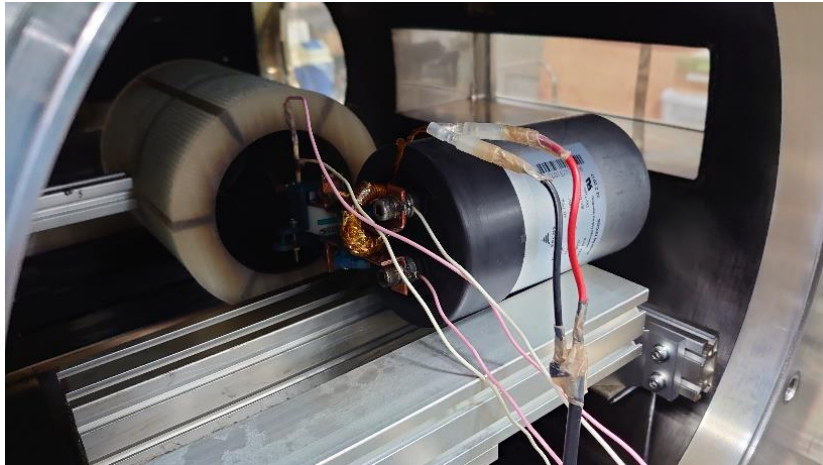


Figure 3.4 Experimental set up appearance from back side

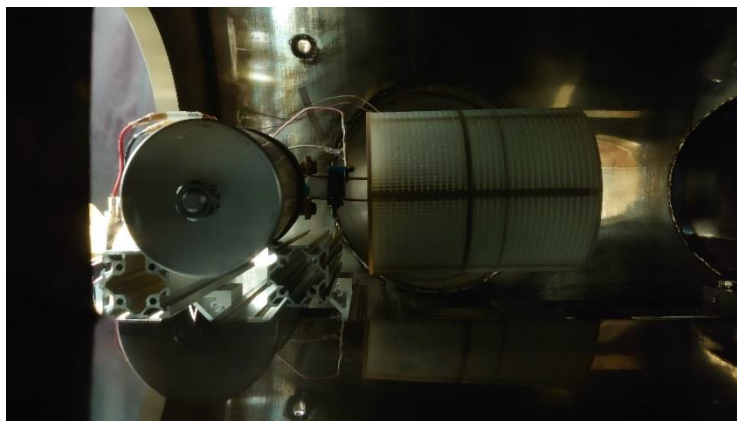


Figure 3.5 Experimental set up appearance from vacuum chamber side window

3.2.2 Result and discussion

Normal PTFE solid propellant was installed, and experiment was carried out with several hundred operations. Figure 3.6 shows the appearance of PPT during discharge. Each number of operation is 902 times at 500 V charge, 1000 times at 750 V charge and 607 times at 1000 V charge. These difference in operation numbers is caused due to

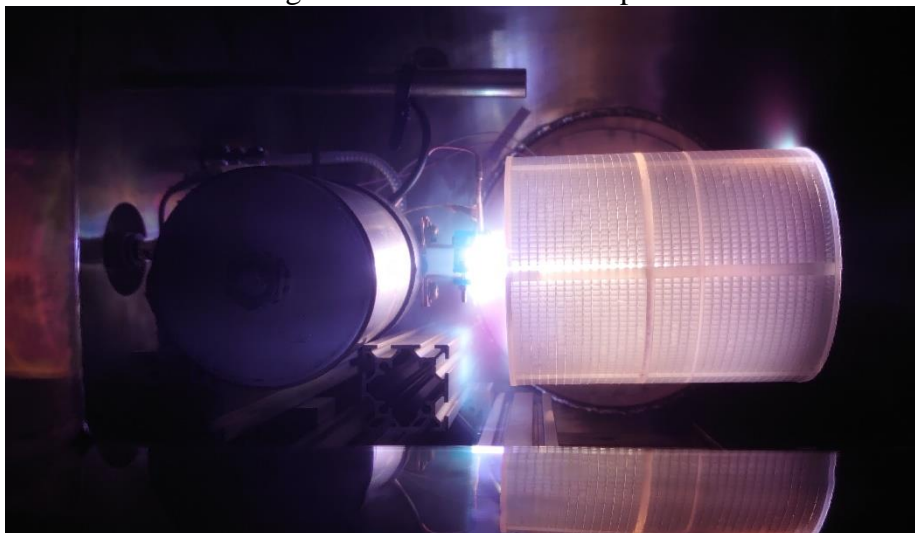


Figure 3.6 PPT appearance during discharge

igniter malfunction. Probably, there are three reasons of this matter, first one is contamination between igniter terminals by the adhesion of carbon which is one of the PTFE component, second one is that supply voltage to igniter was low for experiment vacuum level, and last one is increasing electric resistance due to the Joule heating. For the first reason, igniter tip point, especially inserted part into discharge chamber, was contaminated black stain after experiment. As considering PTFE components, this stain is obviously carbon. This contamination causes discharge difficulty due to electric resistance increasing between terminals or terminals conduction at worst case. This matter might be improved by applying single terminal igniter. This type igniter is mounted only positive terminal on the cathode of discharge chamber and negative side of igniter is connected to its cathode. Since a spark is occurred between the igniter terminal and discharge chamber cathode, a dischargeable area of igniter spark is enlarged and the affection of contamination to igniter is reduced. However, this constitution has a possibility that affection to measure a discharge current by Rogowski coil. Therefore, biaxial terminal igniter is appropriate for this measurement because its circuit is established as one module. The second reason was suggested due to that when the PPT did not work, a little flash at tip of igniter was also not observed in any malfunctions even though operation number was few. The dischargeable voltage in vacuum is extremely higher than the voltage in atmospheric pressure at room. If a voltage of igniter is sufficiently, the flash should be observed between igniter terminals. In this research, we

were not able to prepare a higher voltage supplier, therefore, if we will continue this type research in the future, we must create circuit which can generate ten kV order discharge voltage controlled by MOSFET including capacitor and transformer. For the last reason, we did not measure a temperature of igniter, however, it is presumed by a fact that almost igniter malfunction occurs suddenly after several times continuous operation. Since a contact area of igniter for any other parts is small, the igniter can lower itself temperature by only radiation. Furthermore, even if current value of one operation is small, the operation is performed a plurality of times continuously, so that the next operation is performed before the heat dissipation is completed. In other words, Joule heating of one operation is small, however, temperature increase due to the continuous operation. To improve this matter, a terminals exposed area must be enlarged to increase an amount of heat dissipation by radiation from igniter surface.

The measured impulse bits are shown in Figure 3.7, 3.8 and 3.9. In addition, theoretical impulse bit calculated by measured current are also described in each figure. Impulse bit was measured five times in a row at several operation numbers that are from first operation, from 100 times operation, from 500 times operation. The 750 V charge case was performed after other cases experiment and be measured from first, 500 times and 1000 times operation. The average of measured impulse bit and calculated theoretical impulse bit in each charge voltage are shown in Table 3.1. For Figure 3.7 and 3.8, in either case, the impulse bit decreases as the number of operation increases.

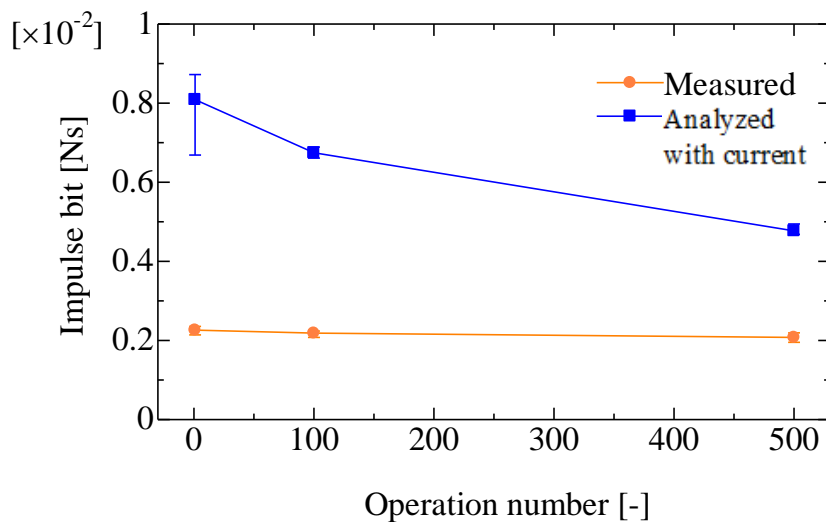


Figure 3.7. Comparison of measured impulse bit and theoretical impulse bit calculated by current data in normal shape solid propellant at 1000 V

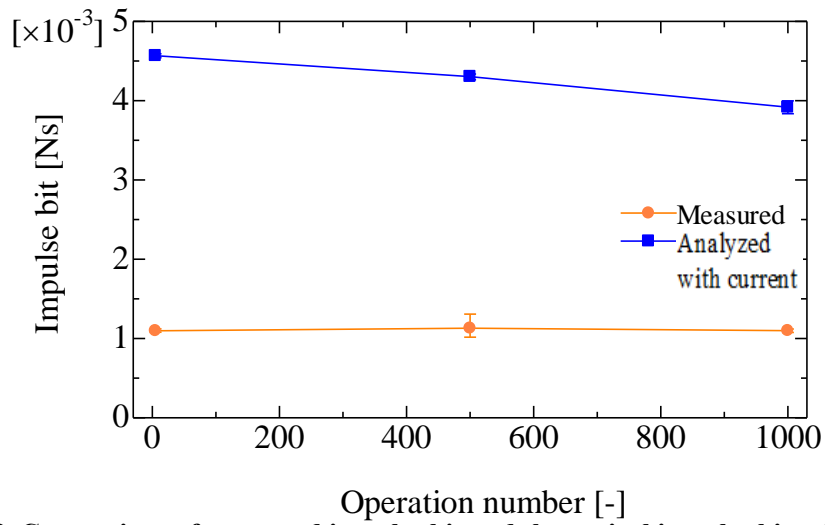


Figure 3.8. Comparison of measured impulse bit and theoretical impulse bit calculated by current data in normal shape solid propellant at 750 V

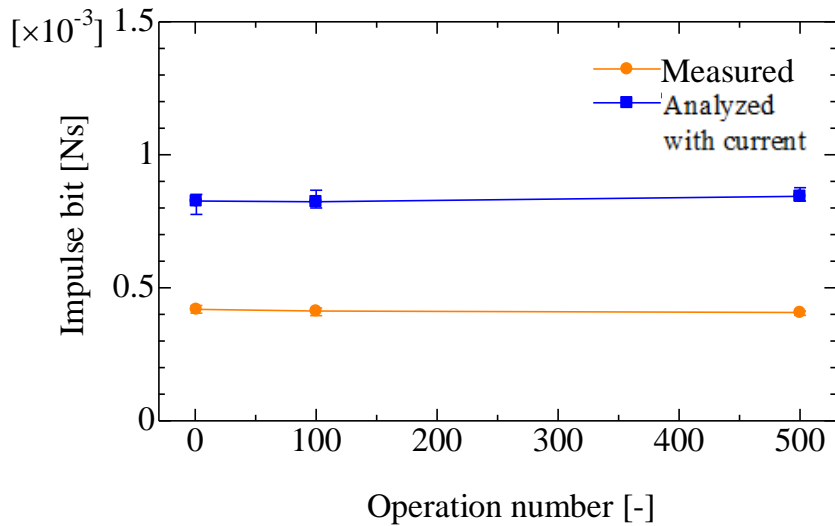


Figure 3.9. Comparison of measured impulse bit and theoretical impulse bit calculated by current data in normal shape solid propellant at 500 V

As can be seen from the Figure 3.9, the surface of the electrode was contaminated with carbon.

Table 3.1. Average values of measured impulse bit and calculated theoretical impulse bit and its ratio

Supply voltage [V]	1000	750	500
Impulse bit average [μ Ns]	2174	1109	411
Theoretical impulse bit average [μ Ns]	6535	4263	831
Ratio of measured value and theoretical one [%]	33.3	26	49.5



Figure 3.10. Anode (upper) and cathode (lower) appearance with contamination of carbon after experiment of normal shape solid propellant

Contamination is more terrible on the cathode (lower electrode in figure). In contrast, anode is contaminated at only the vicinity solid propellant without center. Figure 3.11 shows the maximum current transition. For this graph, the current value decreases as the number of operation times increases. This transition also suggests possibility that the electric resistance value in the discharge circuit is increased. In addition, by the equation (1.63), it is proved that this PPT accelerates and ejects the plasma by the Lorentz force because the measured impulse bit is proportionally supply voltage. The theoretical impulse bit can be calculated with measured current data by equation (1.16), and be also shown in each figure. Tendencies of theoretical impulse bit for operation number are also decreasing in 1000 V and 750 V cases. However, its rate of variation is not similar with measured impulse bit. In only 500 V charge case, it is increased and is also not similar with measured value. In addition, theoretical values are larger from 2 to 5 times than measured value. This fact indicates one possibility that almost electric energy charged in capacitor was wasted as heat energy. An electromagnetic acceleration amount for one particle is limited due to the receivable energy limitation. If supply energy exceeds this limitation, this particle causes further ionization or excitation and absolutes supply energy as internal energy. In other words, almost excessively supply energy for unit mass of

propellant is converted to heat energy and cannot contribute to kinetic energy.

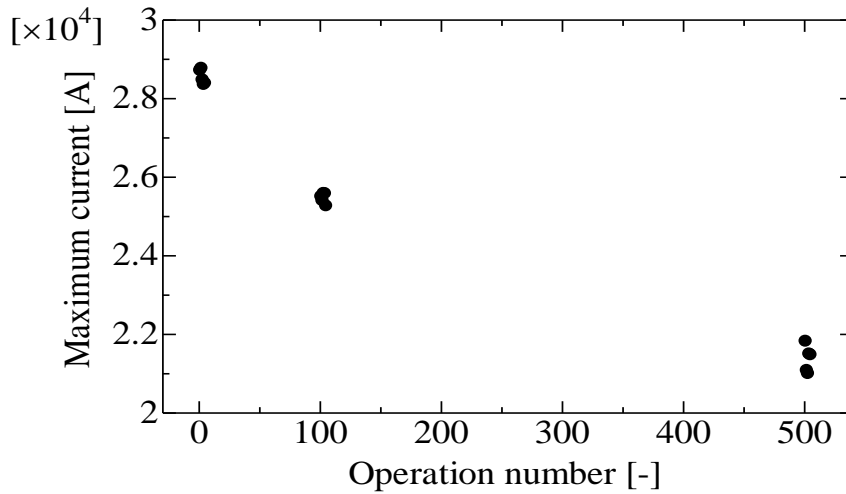


Figure 3.11 Maximum current of normal shape solid propellant at 1000 V

Figure 3.12 shows that the movement of plasma in 2 μ s at 16 μ s after beginning plasma generation. It appears that the current sheet was formed between electrodes and it moves to downstream along electrodes.

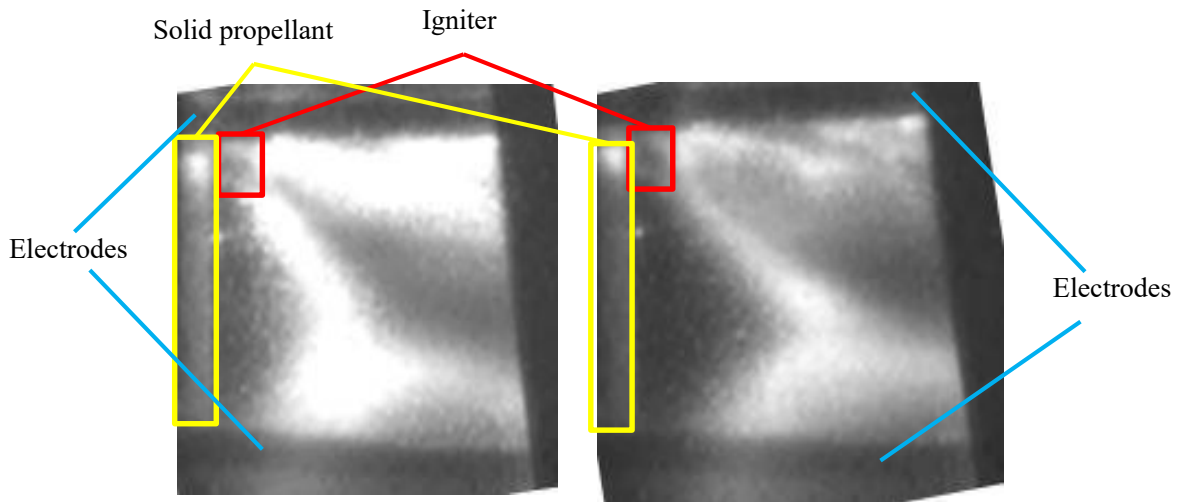


Figure 3.12. Plasma movement for 2 μ s taken with a high-speed camera at 500 V in normal shape solid propellant

Measured consumed mass is shown in Table 3.2 with operation number. The second row of this table shows total consumed mass before and after experiment, and the third row shows that the second row value is divided by operation number in the first row. Due to the different operation number, the total consumed mass with 500 V charge is higher than 1000 V charge by approximately 65 %. For this fact, it can be seen that the mass consumption at one operation increases as the input power increases in normal shape case.

In addition, Table 3.2 also show the calculated momentum coupling coefficient with

related values. The voltage values explained so far are only target values and may differ from the actual values depending on the performance of the power supply unit. Therefore, the voltage value used for such calculation is applied an actual value measured by a high voltage probe. The amount of charged energy in capacitor of the second row is calculated by the input voltage. This momentum coupling coefficient was calculated with this energy and the average of impulse bit. As can be seen from this value, the coefficient of 1000 V charge is highest than others. As a result, the propulsion efficiency increases as the supply energy increase.

Table 3.2. Summary of measured parameters of normal shape solid propellant

	1000V	750V	500V
Operation number	607	1031	902
Consumed mass [g]	0.033	0.04	0.03
Consumed mass per operation number [g]	55.1×10^{-6}	39.3×10^{-6}	33.4×10^{-6}
Actual measured average voltage [V]	976	744	470
Input energy [J]	200	116.2	46.4
Momentum coupling coefficient [Ns/J]	10.9×10^{-6}	9.72×10^{-6}	8.85×10^{-6}

3.3. Perforated solid propellant test

3.3.1 Perforated solid propellant

Figure 3.13 shows perforated solid propellant. Its material is PTFE, and its height, width and depth sizes are the same as for normal solid propellant. There are 5 holes in the height direction at 2 mm intervals, and these holes are 3 rows in the width direction at 2.5 mm intervals. A total of 15 holes are evenly drilled. The hole diameter is 1 mm and its depth is approximately 20 mm. The area of consumption surface is 138.2 mm², which is equivalent to 92.00% of normal shape solid propellant. Therefore, impulse bit will be decreased 8.00 % than normal propellant case. However, consumed mass will be decreased 6.67 % than normal one due to the ratio of propellant surface area which is irradiated radiation.

The procedure of the experiment is the same as that of normal shape. Impulse bit and consumption mass are measured at 500V charge and 1000V charge, respectively. One difference from normal shape case is the processing after cleaning the propellant. Alcohol is used for cleaning with an ultrasonic cleaner before the experiment, however, it may enter into propellant holes and cause an error in mass measurement. Therefore, in the normal shape experiment, the perforated solid propellant after cleaning is left in the vacuum chamber to evaporate and completely remove the attached alcohol. Then, its mass is measured and the experiment is carried out.

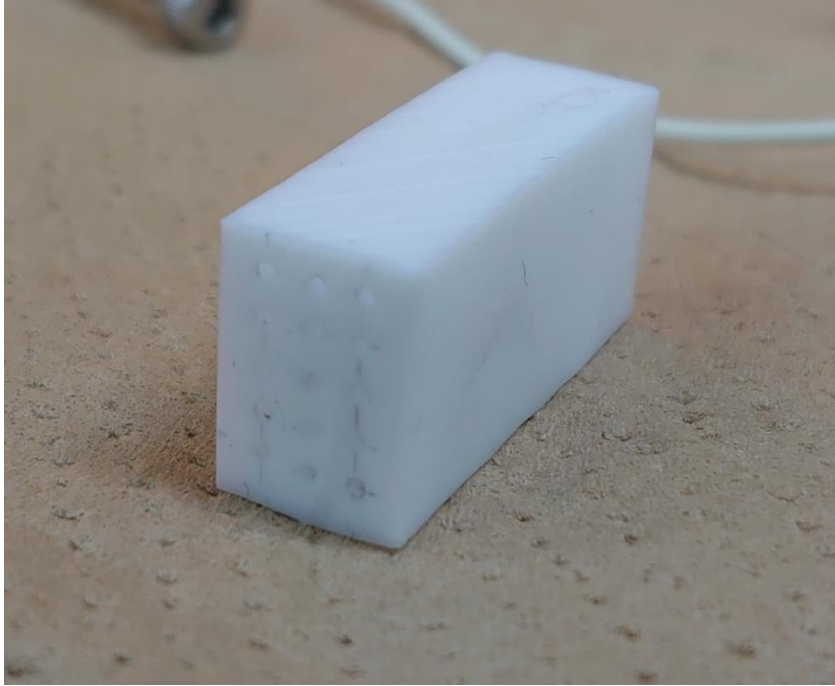


Figure 3.13 Perforated solid propellant

3.3.2 Perforated solid propellant result and discussion

Perforated solid propellant test was also carried out with same supply voltage and condition. Each number of operation is 394 times at 500 V charge, 1000 times at 750 V charge and 607 times at 1000 V charge. The reason of 500 V charge case operation number is less than 500 is igniter malfunction same as normal shape test. However, operation numbers of 1000 V and 750 V charge is purposely adjusted to the operation number of normal shape case.

The each measured impulse bit is shown in Figure 3.14, 3.15 and 3.16. Impulse bit was measured at the same operation number as normal shape experiment.

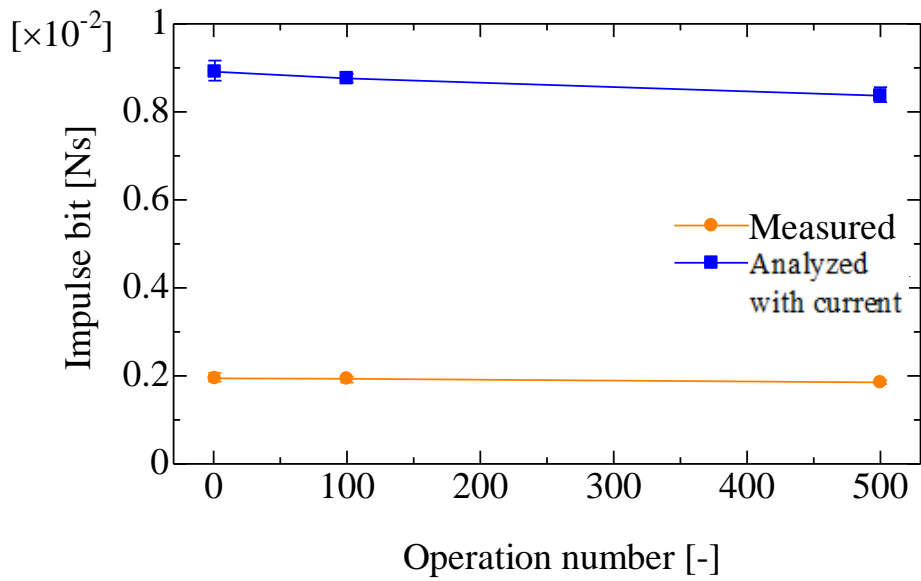


Figure 3.14. Comparison of measured impulse bit and theoretical impulse bit calculated by current data in case of perforated solid propellant at 1000 V

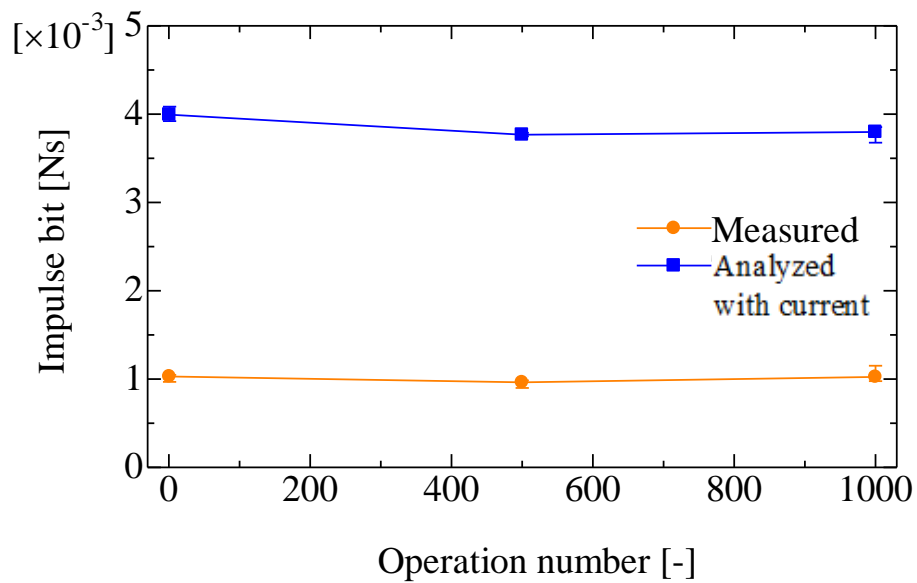


Figure 3.15. Comparison of measured impulse bit and theoretical impulse bit calculated by current data in case of perforated solid propellant at 750 V

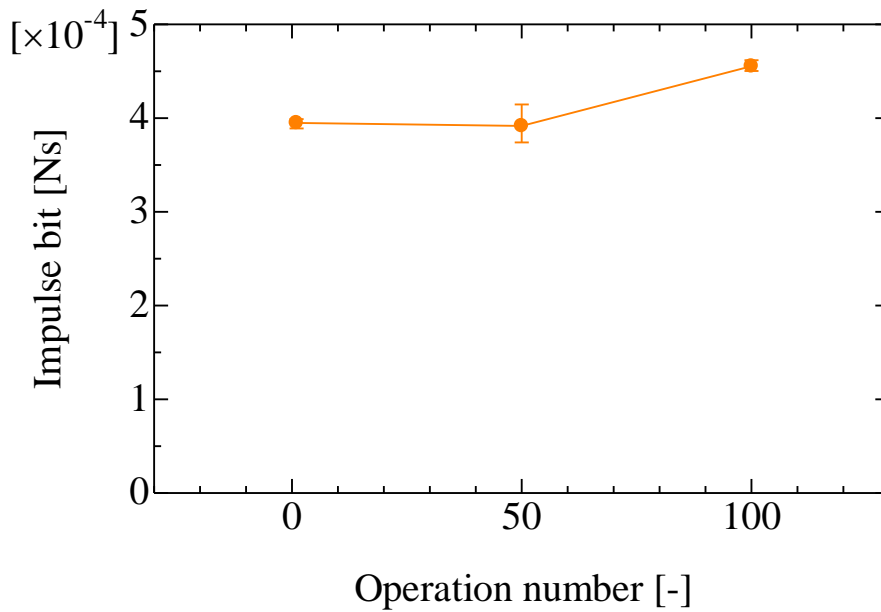


Figure 3.16. Impulse bit of perforated solid propellant at 500 V

However, measurements from 500 times of 500 V charge were not performed due to the malfunction of igniter. Therefore, two impulse bit data from 45 times that was acquired for reference is shown alternatively. The 750 V charge case was performed after other cases experiment and be measured from first, 500 times and 1000 times operation. In addition, theoretical impulse bit is calculated by measured current value and described each graph. However, theoretical value of 500 V charge case was not calculated because it was confirmed that Rogowski coil was removed from PPT electrode after experiment. Therefore, this value is not described. The average of measured impulse bit and calculated theoretical impulse bit in each charge voltage are shown in Table 3.3. In the case of 1000 V

Table 3.3. Average values of measured impulse bit and calculated theoretical impulse bit and its ratio

Supply voltage [V]	1000	750	500
Impulse bit average [μ Ns]	1910	1005	414
Theoretical impulse bit average [μ Ns]	8681	3853	-
Ratio of measured value and theoretical one [%]	22	26.1	-

charge, measured and theoretical impulse bit decrease as the number of operations increases such as normal shape solid propellant results. In the other hand, these values of 750 V case reduced once and increase and become similar value with initial one.

Furthermore, the impulse bit with 500 V charge increases as the operation number increase.

Figure 3.17 shows that the movement of plasma in 2 μs at 16 μs after beginning plasma generation. It appears that the current sheet was formed between electrodes and it moves to downstream along electrodes.

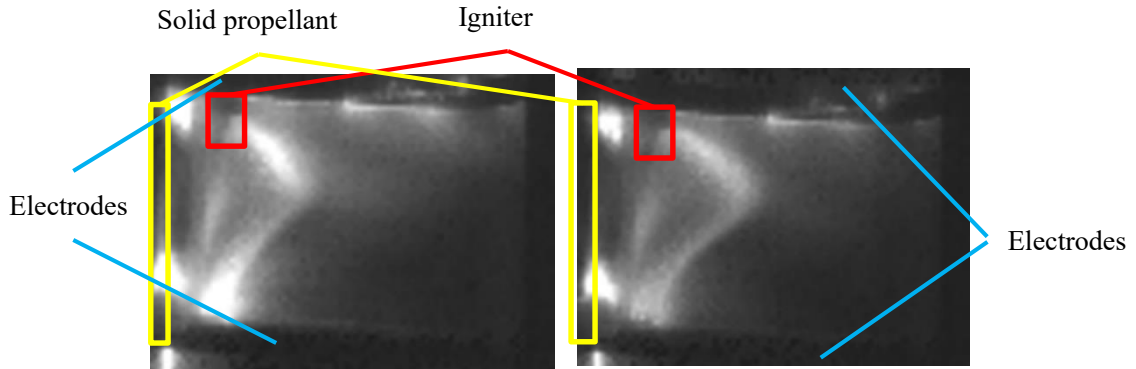


Figure 3.17. Plasma movement for 2 μs taken with a high-speed camera at 500 V in perforated solid propellant

The each consumed mass is shown in Table 3.2 with operation number. This result is also similar to the normal shape solid propellant result, the consumed mass per one operation at 1000 V charge is higher than 500 V charge, and this difference is 158 %.

Furthermore, Table 3.4 also show the calculated momentum coupling coefficient. This value at 1000 V charge is highest. As a different from normal propellant case, momentum coupling coefficient of 750 V case is lowest.

Table 3.4. Summary of measured parameters of perforated solid propellant

	1000V	750V	500V
Operation number	607	1000	394
Consumed mass [g]	0.04	0.05	0.01
Consumed mass per operation number [g]	66.4×10^{-6}	49.3×10^{-6}	25.7×10^{-6}
Actual measured average voltage [V]	968	702	466
Input energy [J]	196.8	103.3	45.6
Momentum coupling coefficient [Ns/J]	9.80×10^{-6}	7.65×10^{-6}	9.08×10^{-6}

For the above results, in the perforated solid propellant case, the relation of supplied power and each parameter such as impulse bit, consumed mass, momentum coupling coefficient is similar with normal shape solid propellant. Furthermore, in the case of 1000V charge, the transition of impulse bit and maximum current versus operation

number also correspond to normal one. In the other hand, in the case of 500 V charge, the transition of impulse bit showed the opposite inclination.

3.3.3 Summary and comparison of perforated and normal shape solid propellant

Up to the previous section, we have examined what kind of tendency is observed in the case of each solid propellant. In this section, the perforated solid propellant results obtained in the previous experiment is compared with normal propellant.

Measured impulse bits are summarized in Figure 3.18. In the 1000V charge case, the overall impulse bit of normal solid propellant higher than perforated one, and which average difference is approximately 12.5 %. Both transitions of impulse bits are very similar in decrease tendency, however, slightly perforated solid propellant is more gradual. In normally, the impulse bit generated by pulsed plasma thruster exponentially decreasing and asymptotically constant. Therefore, this phenomenon will be gently converged. However, if this tendency continues, both impulse bit will be reverse at approximately 2000 times operation. The operation number of PPT usually reaches over tens of thousands in one mission. Thus, perforated solid propellant may be advantageous in over a long period mission because of stability of impulse bit. For 750 V charge case, impulse bits show the opposite tendency each other, however, these values are similar and its difference is 10.3 %. On the other hand, in the 500 V charge case, the impulse bit of normal shape solid propellant is 5.4 % higher than perforated solid propellant in initial part of measurement, however, the impulse bit of perforated solid propellant increases.

The impulse bit of perforated propellant reached in the 100 operation times.

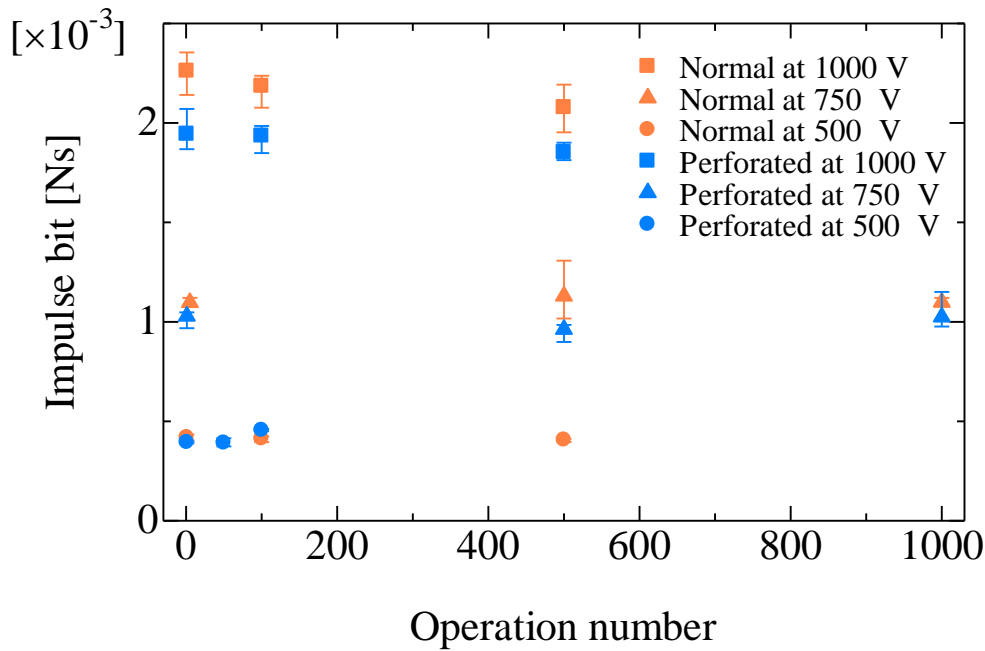


Figure 3.18. Summarized all of measured impulse bit

All of calculated theoretical impulse bit are summarized in Figure 3.19. In contrast to the measured values, perforated propellant with 1000 V charge case is highest. On the other hand, the difference of 750 V case is 10.6 %, and this percentage is similar with measured value. Since theoretical impulse bits are calculated by measured current value, these facts indicate that an amount of total current of perforated propellant is supplied excessively.

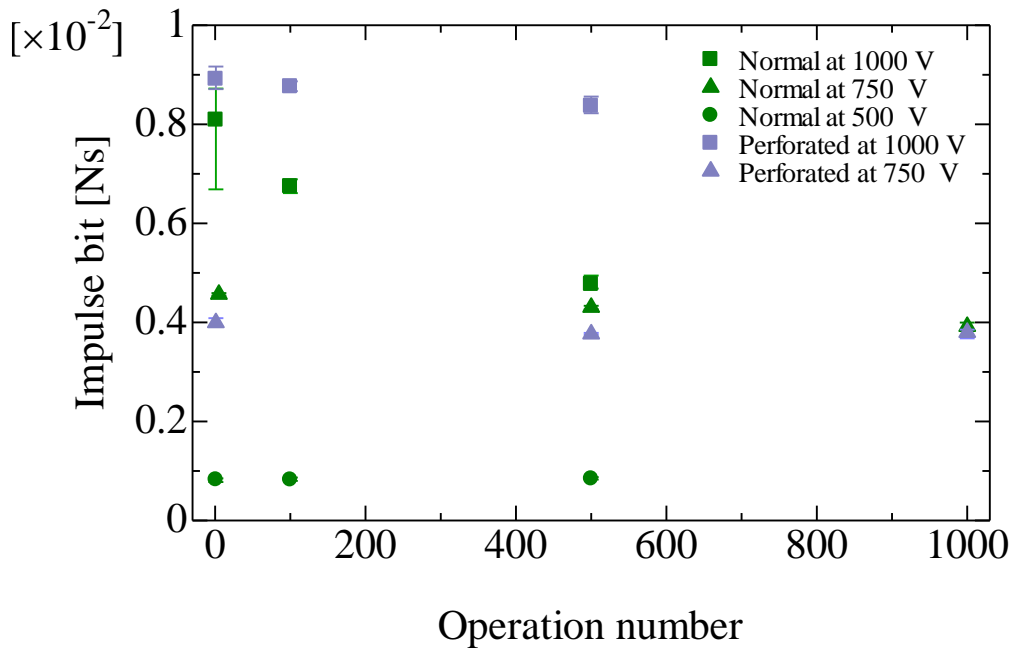


Figure 3.19. Summarized all of calculated theoretical impulse bit transition

Figure 3.20 shows momentum coupling coefficient of each condition. For these values, performances of all supply voltage and shape can be compared. Transitions of the coefficient in the case of normal shape solid propellant at all voltages and perforated one at 1000 V decreased. In contrast, the transition of perforated solid propellant of 500 V case and normal propellant of 750 V case increased. In the case of perforated solid propellant at 750 V charge, it decreased once and increased finally. The highest value is normal shape solid propellant with 1000 V charge, however, assuming that the tendency of perforated propellant with 500 V charge does not change, it will exceed at approximately 180 operation times.

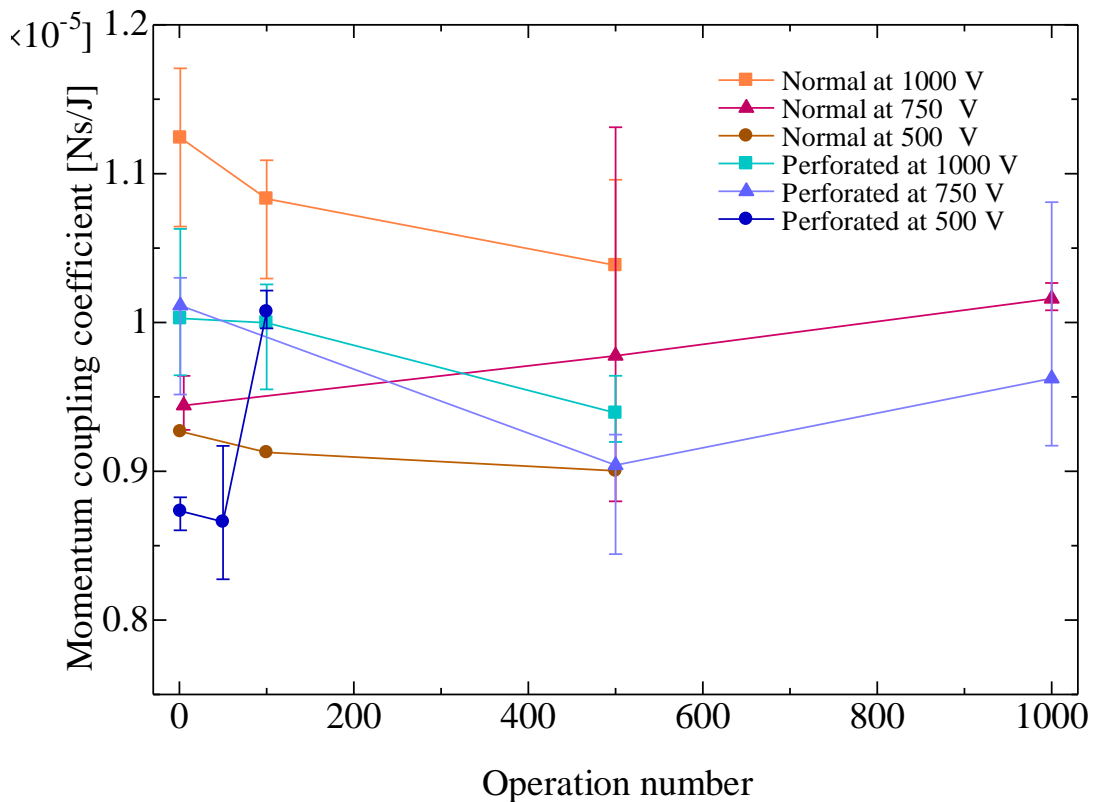


Figure 3.20. Comparison of momentum coupling coefficient

The data of consumed mass per one operation are shown in Figure 3.21. When 1000 V is applied, the amount of consumption in the case of normal propellant is 17 % lower than another one. In the case of 750 V charge, similar as 1000 V charge case, consumed mass of normal propellant is lower than perforated one, and its difference is 20.3 %. In contrast, when 500 V is applied, the consumption of perforated propellant case is 23 % lower. This fact indicates the possibility that the ideal solid propellant shape exists depending on supplied energy.

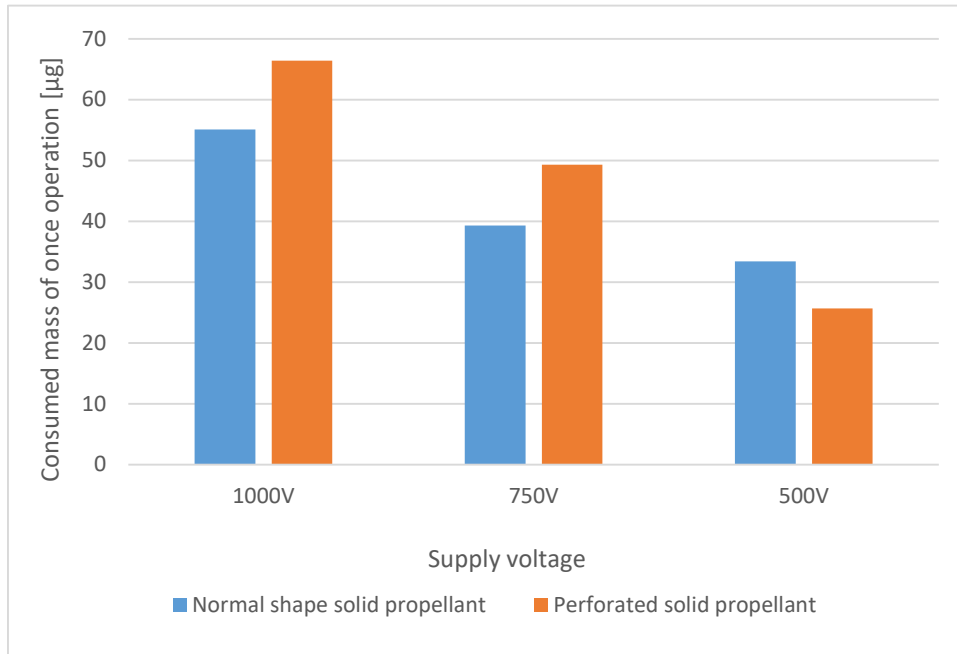


Figure 3.21. Comparison of consumed mass per one operation

Figure 3.22 and 3.23 shows one kind of the frequency distribution examples. These distribution graphs are classified by dividing from maximum value to minimum value by 10. As can be seen in these two figures, impulse bits of this experiment PPT are inclined toward maximum value. This distribution indicates possibility that this PPT cannot be evaluated simply by average value. Therefore, if we want to evaluate the PPT performance in the future, evaluation should be carried out with maximum value and minimum value.

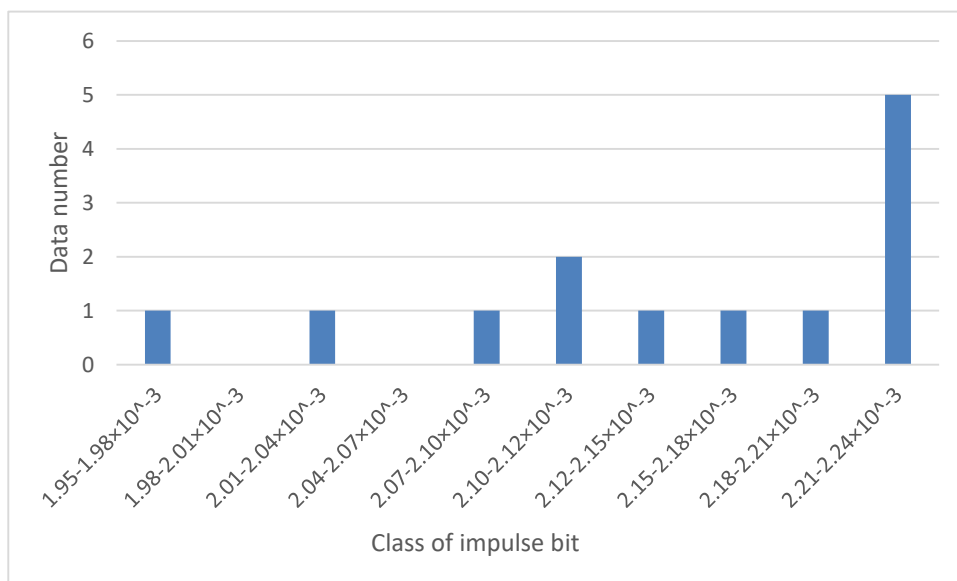


Figure 3.22. Frequency distribution example (the case of normal solid propellant with 1000 V charge)

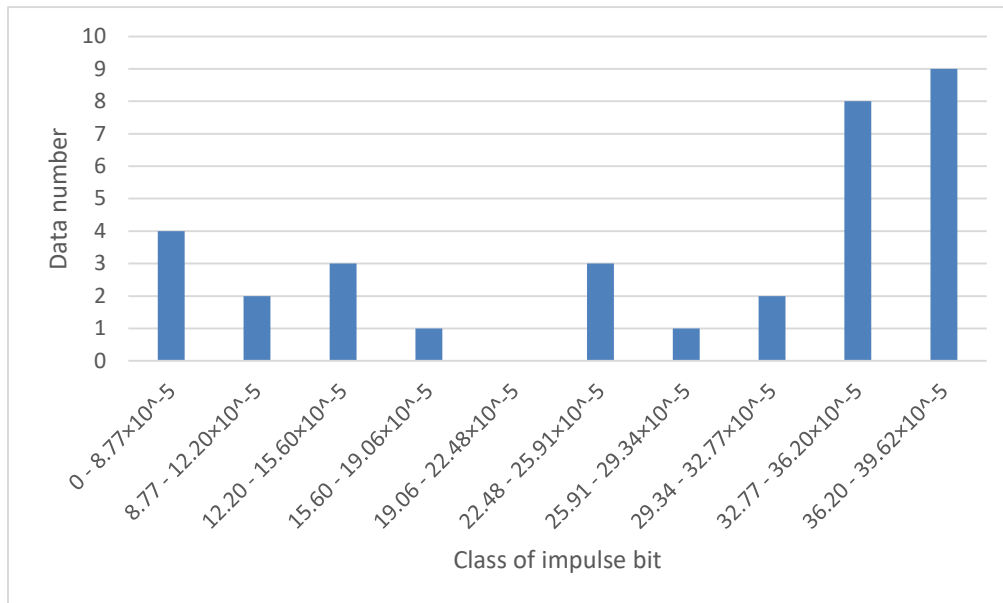


Figure 3.23. Frequency distribution example (the case of perforated solid propellant with 500 V charge)

For above facts, we can suppose one possibility that high effective electromagnetic acceleration was performed in perforated solid propellant case with 500 V supply. Naturally, if consumed surface area is decreased, consumed mass should also be decreased. In addition, although theoretical impulse bits (which is calculated by current) of perforated propellant are same or moreover than normal propellant, actual measured value of perforated one is lower. These facts probably indicate that electric energy was supplied excessively in perforated solid propellant case of 1000 V and 750 V charge because supply energy was same with normal propellant though consumed mass was decreased. As a result, excessively supply energy was consumed as internal energy and converted heat energy, thus it cannot contribute to electromagnetic acceleration. Furthermore, this heat energy generate radiation, and since it urged sublimation of solid propellant by LTA, consumed mass per operation was increased. In the other hand, in the case of 500 V charge, since supply energy was properly increased not to exceed until limitation that each propellant particle can convert to kinetic energy, the impulse bit was higher than normal shape solid propellant. Furthermore, for this reason, consumed mass of perforated propellant was less than normal propellant because supply propellant mass in perforated propellant case (which particles generate radiation energy) was lower.

Therefore, if the capacity of the capacitor is reduced to reduce the amount of total electric energy or the total consumed mass area of the solid propellant is increased, the performance as in the case of applying 500 V might be obtained even at a high voltage.

Chapter 4: Conclusion

In order to gain a clue to improving the performance of Ablation-Fed Pulsed Plasma Thruster, which is one kind of electric propulsion unit with solid propellant, the performance of proceeded solid propellant, which is a new approach method, was verified. Verification was carried out experimentally with comparison of normal shape solid propellant and perforated solid propellant (perforated perpendicular to the consumption surface). Each propellant was evaluated with three supply energy conditions (1000 V, 750 V and 500 V charge) by impulse bit measured with thruster stand, theoretical impulse bit calculated by measured current value, consumed mass and momentum coupling coefficient.

Firstly, we succeeded to operate PPT with perforated solid propellant and to measure the impulse bit of that with thruster stand. In addition, discharge current from main capacitor in PPT electrode was also measured with Rogowski coil.

Overall, the normal shape solid propellant with 1000 V charge indicated highest thrust performance in impulse bit and momentum coupling coefficient. However, in the case of perforated solid propellant, the characteristic properties that might exceed normal propellant performance were obtained. At first, the transition of impulse bit. In the 1000 V charge experiment, impulse bit tended to decrease for both propellants. However, the tendency of perforated propellant is gentler, and if that tendency continues, the impulse bit of perforated propellant will exceed after approximately 2000 operations. This tendency is also indicated in the momentum coupling coefficient. On the other hand, the most characteristic result was obtained in the case of perforated solid propellant with 500 V charge. The normal propellant was similar to other voltages, and the transition of impulse bit decreased. In contrast, perforated solid propellant with 500 V charge showed the increasing tendency of impulse bit and momentum coupling coefficient. Although it was lower than normal propellant at few times of operation, the impulse bit equivalent to normal propellant was generated at 100 operations. In this experiment, unfortunately, the measurement more operation times than this was not carried out due to the malfunction of igniter, however, the possibility of impulse bit increasing was suggested.

Also in the result of consumed mass, perforated solid propellant with 500 V charge indicated interesting property. In the case of 1000 and 750 V charge, the consumed mass of normal propellant is lower than perforated propellant, however, at 500 V charge, the perforated propellant consumed mass was lower than the another. This difference in consumed mass is 30.0 %, and this value can be supposed critical because the average impulse bit of perforated propellant is 5.4 % lower than normal one.

For all of above results, almost supply electric energy was converted to heat energy at 750 and 1000 V charge due to the excessive energy for solid propellant supply. Therefore, even at high supply voltage, the performance similar to a 500 V charge

perforated solid propellant might be obtained if the capacity of capacitor is decreased and total supply energy is reduced.

In the ablation-fed solid propellant pulsed plasma thruster, it is the general idea that propellant is mounted as much as possible to eliminate waste. However, as shown in the result of this research, the solid propellant might have an optimal shape depending on the operating supply power. Hence, it is necessary further verification of the hole shape, size and position.

REFERENCES

- [1]. Keiichi K. Yoshihiro A. Introduction to Electric Propulsion. Japan: University of Tokyo Press, 2003: 1-65, 157-178.
- [2]. Shigeaki U. Laser propulsion [J]. Fusion Plasma, 2005, 81: 186-194.
- [3]. Y ARAKAWA. REVIEW OF ELECTRIC PROPULSION ACTIVITIES IN JAPAN. USA, Seattle: International Electric Propulsion Conference . 1993
- [4]. OneWeb LLC. Oneweb Network Update. [2019-12-9].
<https://www.oneweb.world/technology#video>.
- [5]. William J. Guman and Paul E Peko. Solid-Propellant Pulsed Plasma Microthruster Studies, June 1968.
- [6]. R. L. Burton and P.J. Turchi. Pulsed Plasma Thruster. JOURNAL of PROPULSION AND POWER, 1998, Volume 14 (Issue No. 5): 716-735.
- [7]. Ryu F. PROCYON Ultra-small satellite for deep space exploration, The university of Tokyo and JAXA, 2014
- [8]. J. M. Sankovic. Ultra-Low-Power Arcjet Thruster Performance. NASA TM 106400, Nov. 1993.
- [9]. Nikolay N A. Garry A P. Michael N K. Ablative pulsed Plasma Thruster R&D in Russia since the Beginning of the 90s. USA. Washington D.C: 33th International Electric Propulsion Conference, 2013.
- [10]. Thomassen K and Solbesj A. Analysis of solid teflon pulsed plasma thruster, Journal of Spacecrafts and Rockets, 6,565–569 (1969)
- [11]. Matthew S. Joshua L. Observation of Late-Time Ablation in Electric Solid Propellant Pulsed Microthrusters. UT. Salt Lake: Propulsion and Energy Forum. 2016

- [12]. Spanjers Gregory G and McFall Keith A and Gulczinski F SIII and Spores Ronald A. Investigation of propellant inefficiencies in a pulsed plasma thruster, AIAA paper, 96, 2723 (1996)
- [13]. Robert G. Physics of Electric Propulsion. MCGRAW-HILL BOOK COMPANY, 1968
- [14]. Satoshi K. The study of pulsed plasma thruster with liquid propellant. Tokyo : Tokyo University, 2003
- [15]. Masakatu N. Akira K. Simple calibration method of thruster stand. The study bulletin by Tokyo Metropolitan College of Industrial Technology Arakawa campus , 2016, 10: 45-49.
- [16]. Keisuke T. Shinya M. Daijiro Y. Hiroki W. Haruka T. Development of Thrust Target for Evaluation 100 μ Ns Level Impulse Bit. Japan.: Proceedings of Space Transportation Symposium FY2014, 2014
- [17]. Thomas E. Markusic and Ronald A. Spores. Spectroscopic Emission Measurements of a Pulsed Plasma Thruster Plume. Vol. AIAA 97-2924, 1997.
- [18]. Isamu F. Naoji Y. The basic study of electromagnetic acceleration propulsion unit with ionic liquid propellant. 2016
- [19]. Tony S. Anusche N. Matthias L. Dejan P and Georg H. Review of Pulsed Plasma Thruster Development at IRS. Japan: JSASS Aerospace Tech, 2010.
- [20]. Lynn A. Tom W. Nicole J. A Performance Comparison of Pulsed Plasma Thruster Electrode Configurations. USA. Ohio: 25th International Electric Propulsion Conference, 1997
- [21]. Guman W J. Pulsed Plasma Technology in Microthrusters. Fairchild Hiller Corp. Farmingdale. NY. 1968.

- [22]. M Coletti. R I Marques. S B Gabriel. Design of a Two-Stage PPT for Cubesat Application. USA. Michigan: 31th International Electric Propulsion Conference, 2009
- [23]. Naohiro T. Ryoichi A. Yuko H. Nozomi T. Akira A. Alfvén critical velocity in plasma acceleration by magnetic nozzle. Tohoku university
- [24]. M Lau. G Herdrich. Pulsed Plasma Thruster Endurance Operation Stress Testing at IRS. USA. Washinton D.C: 33rd International Electric Propulsion Conference, 2013
- [25]. Kazuki M. Naoji Y. Taichi M. The verification of the air suction type electromagnetic acceleration unit. Japan: Fukuoka. Kyushu University. 2018
- [26]. Isamu F. Naoji Y. The fundamental study of electromagnetic acceleration with ionic liquid propellant. Japan: Fukuoka. Kyushu University. 2017
- [27]. Mizuki K. Yuji O. Nao A. Taishi H. Hideyuki H. The repetition performance of laser assist pulsed plasma thruster. Japan. JAXA.
- [28]. NASA. Specific Impulse. [2015-05-05]. <https://www.grc.nasa.gov/WWW/K-12/airplane/specimp.html>.
- [29]. Kaartikey M. Multiple Plasma Stream Electromechanical Model for Pulsed Plasma. India. Manipal. Manipal Institute of Technology. 23 April. 2018
- [30]. Francis F. Chen. Introduction to Plasma Physics and Controlled Fusion. Germany. Springer, 2015: 1-178.
- [31]. Kenrou M. The fundamental plasma physics. Japan. Iwanami Shoten, Publishers. 1997

ACKNOWLEDGEMENTS

I would like to thank Prof. Naoji Yamamoto who provided helpful comments and suggestions.

I am also indebt to Dr. Hu Jing whose comments made enormous contribution to my paper.

My completion of this thesis could not have been accomplished without the support of Prof. Wang Dong.

I also express my deep thanks to Kouichi Ushio, Masakazu Otubo, Kaartikey Misra, Misaki Adachi, Shintaro Miyata for their kind support and advice.